

On the development and analysis of coupled surface-subsurface models of catchments.

Part 3. Analytical solutions and scaling laws

Piotr Morawiecki[†] and Philippe H. Trinh[‡]

Department of Mathematical Sciences, University of Bath, Bath BA2 7AY, UK

(Received xx; revised xx; accepted xx)

The objective of this three-part work is the formulation and rigorous analysis of a number of reduced mathematical models that are nevertheless capable of describing the hydrology at the scale of a river basin (i.e. catchment). Coupled effects of surface and subsurface flows are considered.

In this third part, we focus on the development of analytical solutions and scaling laws for a benchmark catchment model that models the river flow (runoff) generated during a single rainfall. We demonstrate that for catchments characterised by a shallow impenetrable bedrock, the shallow-water approximation allows a reduction of the governing formulation to a coupled system of one-dimensional time-dependent equations for the surface and subsurface flows. Asymptotic analysis is used to derive semi-analytical solutions of the model. We provide simple asymptotic scaling laws describing the peak flow formation. These scaling laws can be used as an analytical benchmark for assessing the validity of other physical, conceptual, or statistical models of catchments.

1. Introduction

In this third and final part of our work, we leverage the parametric study (Part 1, [Morawiecki and Trinh 2022a](#)) and two-dimensional benchmark models (Part 2, [Morawiecki and Trinh 2022b](#)) in order to perform an in-depth asymptotic analysis of a coupled surface-subsurface model of a catchment. The specific situation we consider is flow within an overland-dominated aquifer, characterised by a thin layer of soil. The system begins in a steady state (set to a constant rainfall), and is then subjected to intense rainfall.

One of the primary results we derive is that the river flow in such a situation rapidly saturates to

$$Q_{\text{crit}} = \underbrace{K_s S_x L_z}_{\text{groundwater flow}} + r L_x \underbrace{\left(1 - \frac{K_s S_x L_z}{r_0 L_x}\right)}_{\text{overland flow}}, \quad (1.1)$$

which is composed of a contribution due to the subsurface/groundwater flow, and a contribution due to the overland flow over an already saturated region. The parameters L_x , L_z , and S_x relate to geometrical features of the hillslope, while K_s corresponds to the soil hydraulic conductivity, and r the rainfall intensity.

As we argue in this work, such analytical scaling laws are valuable, both as a tool to diagnose the correctness of other (more complex) rainfall-runoff models, and also as a measure in characterising a catchment's propensity to flooding.

The introduction of Part 1 covers the general subject of hydrology and parameter

[†] Email address for correspondence: pwm27@bath.ac.uk

[‡] Email address for correspondence: p.trinh@bath.ac.uk

estimation, while the introduction of Part 2 covers computational rainfall-runoff models. We begin by discussing the importance of this particular work, focusing on asymptotics and scaling laws, in the context of the existing literature.

1.1. *On the importance of analytical benchmarks results*

Catchment hydrology is one of many areas of engineering in which numerical approaches seem to dominate over analytical ones. Owing to the complex multi-scale nature of hydrology, limited data availability and high computational cost, it can be enormously challenging to formulate and solve the correct equations (Grayson et al. 1992). Often, instead of physical models based on fundamental laws of hydrodynamics, simpler models are used to describe flow formation; these include e.g. conceptual and statistical models (Moore et al. 2007). Typically, these models are formulated using a trial-and-error-based approach, so as to fit available real-world data. However, such approaches do not provide any guarantee of model performance when applied to situations that may be underrepresented or missing in the training datasets (Beven 2018; Parkin et al. 1996; Bathurst et al. 2004).

In order to better understand the theoretical limits of different classes of catchment models, it is crucial to have a firm analytical understanding of the different processes characterising the physical models. This can be done by developing numerical benchmark scenarios, like in the work of e.g. by Sulis et al. (2010) and Maxwell et al. (2014), and using them to compare predictions of different models. One perspective is that, in order to guarantee consistency between the models over a wide range of input parameters, models should predict the same scaling laws for key features. For instance, consider a model that predicts that the river flow, Q , is proportional to the catchment area, A , so $Q \propto A$; in contrast, a second model predicts that $Q \propto \sqrt{A}$. Then disregarding the fitting of these models, they cannot give consistent predictions over the whole range of A values. For example, the second model fitted to a training dataset dominated with measurements conducted in large catchments would tend to overestimate flow in the case of small, often ungauged catchments. This perspective seems oversimplistic, but we argue that such asymptotic scaling laws are not entirely well-established in modern hydrology.

The emphasis of our work, here, is the derivation of such analytical scaling laws for flow prediction for the case of coupled surface-subsurface flows in catchments. Not only do such scaling laws provide clear guidance on the key dependencies of model parameters, but their analysis will often illuminate further model simplifications.

We next provide a brief overview of the existing analytical theory, emphasising the lack of research on fully-coupled surface-subsurface systems.

1.2. *On analytic solutions in catchment hydrology*

The typical governing equations used in physical catchment models includes Richards equation for the subsurface flow (or the Boussinesq equation for the saturated groundwater flow) and the Saint Venant equations for the overland and channel flows [see e.g. the review by Shaw et al. (2010)]. These equations and their simplifications have been well-studied using analytical methods, though largely in an uncoupled manner. For instance, in the case of the groundwater flow, the Boussinesq equation is commonly used to determine the shape of the groundwater table (Hálek and Švec 2011, chap. 2); in some cases analytical solutions can be derived. This includes, e.g. steady-state groundwater flow and evolution in one-dimensional hillslopes (Polubarnova-Kochina and Wiest 1962; Troch et al. 2013). Similarly, analytic solutions have been developed for the 1D Richards equation in order to describe water transfer through the unsaturated soil under constant and time-varying infiltration (Warrick et al. 1990).

For the case of overland flow over a hillslope, analytical solutions have been given by a kinematic approximation of the Saint Venant equations by e.g. [Parlange et al. \(1981\)](#) and [Tao et al. \(2018\)](#). Such analytic solutions and their approximations are important, since they provide benchmark models for testing numerical schemes (e.g. benchmarks by [MacDonald et al. \(1995\)](#) for the overland flow and by [Tracy \(2006\)](#) for the subsurface flow), and may be used to develop less computationally demanding modelling approaches such as TOPMODEL by [Kirkby and Beven \(1979\)](#). Nevertheless, analytical solutions have not been found so far in the case of coupled systems including governing equations describing both subsurface/groundwater and surface flow—despite the importance of these models in catchment hydrology, the study of these models has been restricted to numerical solutions only ([Maxwell et al. 2014](#)).

1.3. On the shallow water approximation for subsurface flow

Previously in Part 2, we introduced two benchmark scenarios. *Scenario A* was introduced to describe a catchment with a deep aquifer (including both soil and a well-conducting deep bedrock layer); while *Scenario B* describes a catchment where the subsurface flow is predominantly transferred through a thin layer of soil. Mathematically, Scenario B is the limiting case of Scenario A in which aquifer depth is much smaller than catchment width, $L_z \ll L_x$. We showed that in both cases, under standard initial conditions, the full three-dimensional catchment model can be reduced, to leading-order, to a simpler two-dimensional hillslope model. We shall begin with this two-dimensional assumption as a basis in this paper. We then demonstrate that in Scenario B, under certain assumptions, the two-dimensional model can be further reduced to a one-dimensional model.

Reduction of the two-dimensional subsurface flow into a one-dimensional model is not a new concept. The simplification is based on the Dupuit-Forchheimer approximation by [Dupuit \(1863\)](#) and [Forchheimer \(1914\)](#), which states that the groundwater flow is predominantly horizontal, and that the total flow scales proportionally with the saturated aquifer thickness. [Boussinesq \(1877\)](#) used this assumption to develop a one-dimensional PDE for the groundwater height $H(x, t)$ known as the Boussinesq equation. As we show later, it can be derived from the 2D Richards model under the aforementioned assumption that $L_z \ll L_x$. The accuracy of this approximation is studied in detail by [Paniconi et al. \(2003\)](#) and [Cook et al. \(2009\)](#).

The Boussinesq equation is commonly used in the groundwater modelling, and a wide class of analytic and approximate solutions have been developed. Notable examples are reviewed by [Wooding and Chapman \(1966\)](#), [Anderson and Brooks \(1996\)](#), [Troc et al. \(2003\)](#), and [Bartlett and Porporato \(2018\)](#). These studies, however, concern only groundwater flow, and do not involve the coupling with the overland flow, which is an essential component of a standard physical catchment model.

Here, we extend these studies by including the effect of overland flow in the Boussinesq equation. Our main result in this paper is the derivation and analysis of the following one-dimensional coupled surface/subsurface model:

$$\frac{\partial H}{\partial t} = \begin{cases} f(x)^{-1} \left[\frac{\partial}{\partial x} (\sigma H \frac{\partial H}{\partial x} + H) + \rho_0 r(x, t) \right] & \text{if } H \leq 1, \\ \frac{\partial}{\partial x} \left(\sigma \frac{\partial H}{\partial x} + \mu \sqrt{1 + \sigma \frac{\partial H}{\partial x}} (H - 1)^k \right) + \rho_0 r(x, t) & \text{if } H > 1. \end{cases}$$

where $f(x)$, σ , μ and ρ_0 are dimensionless parameters explained in detail in section 2.3, and $H(x, t)$ is total height of groundwater and surface water, with $H \leq 1$ representing unsaturated soil without surface water, and $H > 1$ saturated soil with surface water. The

main difference from the classical Boussinesq equation is the second case, in which we include an additional term representing the overland flow.

We shall use the above one-dimensional coupled surface-subsurface model in order to develop analytical solutions for the river flow formed by rainfall of a constant intensity (however, the result can be generalised for time-dependent rainfall). Our methodology, which uses the method of characteristics for the study of wave propagation is similar to previous kinematic treatments of the Saint Venant equations (Woolhiser and Liggett 1967; Henderson and Wooding 1964), but for our problem, the size of the saturated zone increases as a result of rising groundwater, and this introduces secondary dynamics.

The analytical approximations we develop in this work are possible due to a few governing assumptions; these are strongly supported by the analysis of the typical values of catchment parameters described in Part 1 (Morawiecki and Trinh 2022a). The main approximations are: (i) the typical rainfall duration is much shorter than the characteristic timescale of groundwater flow; (ii) the typical timescale of surface flow is much shorter than subsurface flow; and (iii) the mean precipitation rate is larger than the maximal groundwater flow passing through the saturated zone.

We start by introducing the above one-dimensional model in §2, with its typical dynamics discussed in §3. For a scenario of single intensive rainfall described in §4, we find approximated analytic form of the initial steady state in §5, followed by short-time asymptotic analysis in §6. The accuracy of developed analytic approximations is assessed in §7. In §8 we highlight key hydrograph features predicted by this analytic solution, followed by conclusions in §9 and further discussion in §10.

2. Formulation of the one-dimensional coupled model

In this section, we introduce a one-dimensional model describing the horizontal groundwater and overland flow along the hillslope, firstly in a dimensional and then in a dimensionless form. Its formal mathematical derivation from the two-dimensional benchmark model introduced in our previous paper is presented in appendix B — here we focus on presenting the general structure of the model instead.

2.1. Dimensional model

Let us consider a two-dimensional hillslope of length L_x with uniform slope S_x , uniform soil depth L_z , uniform saturated soil hydraulic conductivity K_s , and with an impenetrable bedrock beneath the hillslope. As shown in the (x, z) -plane in fig. 1, we denote the depth of the saturated zone as $H_g(x, t)$, and the height of the surface water as $h_s(x, t)$.

We shall assume that overland flow can only occur when the soil becomes fully saturated (known as the *Horton overland flow*), which occurs when the rainfall exceeds the soil infiltration capacity (Kirkby 2019). The overland flow generated by exceeding the soil infiltration capacity is not considered. Under this assumption, the heights, H_g and h_s , can be combined to form a single dependent variable,

$$H(x, t) = H_g(x, t) + h_s(x, t), \quad (2.1)$$

defined as the total height of groundwater and surface water. We now review the governing equations for H , for which the details are presented in appendix B.

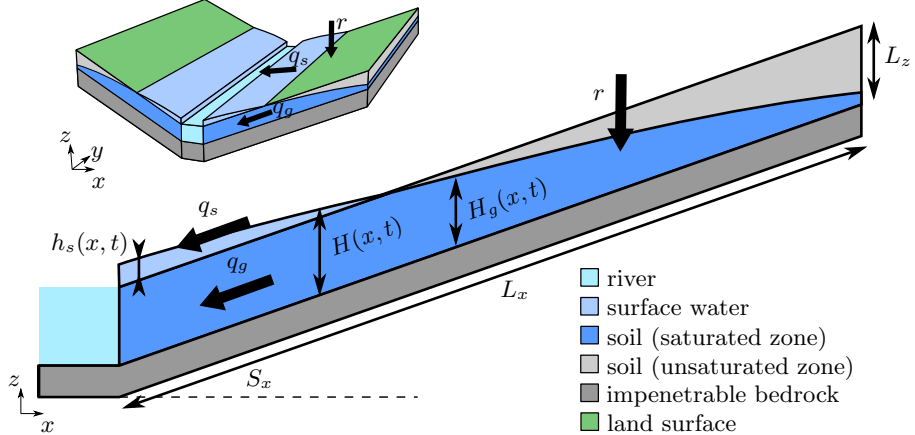


Figure 1: Hillslope geometry used to formulate a 1D surface-subsurface model.

2.1.1. Groundwater flow

Note that the groundwater flow, considered under the standard Dupuit assumptions, is given by

$$Q_g = K_s H \frac{\partial H}{\partial x} + K_s H S_x. \quad (2.2)$$

When the soil is not fully saturated, and hence $H < L_z$, the evolution of the groundwater depth is given by the continuity equation, resulting in a standard form of Boussinesq equation (Boussinesq 1877):

$$f(x, t) \frac{\partial H_g}{\partial t} = \frac{\partial}{\partial x} Q_g + r = \frac{\partial}{\partial x} \left(K_s H_g \frac{\partial H_g}{\partial x} + K_s H_g S_x \right) + r(x, t), \quad (2.3)$$

where $r(x, t)$ denotes the groundwater recharge and $f(x, t)$ is a drainable porosity. In the paper, we assumed that the recharge is equal to the precipitation.

The drainable porosity function is more subtle; as first introduced in appendix B, it is formally defined as the rate of change of groundwater volume \mathcal{V} given a change in the groundwater level, H , *i.e.* $f = d\mathcal{V} / dH$. In the literature [e.g. Troch et al. 2003] it is often assumed to be a constant parameter characterising each given soil type. In general however, it depends on the saturation profile, $\theta(h)$, above the groundwater, which rapidly changes as the rainfall infiltrates through the partially saturated sections of the soil; this is observed in the full two-dimensional solutions presented in the previous part of our work.

Instead, in this paper, we use a mean drainable porosity computed at the initial state, and defined via

$$f(x, t) = f(x) = \frac{v_H(x)}{D(x)}, \quad (2.4)$$

where $v_H(x)$ is the initial drainable volume per unit area at a given location, and $D(x) = L_z - H(x)$ is the depth of the groundwater below the land surface. In other words, drainable porosity is given by the fraction of the soil volume that can be filled with water. Taking the mean porosity does not fully reproduce the groundwater table growth dynamics, but correctly predicts that the entire column of soil becomes fully saturated. Further discussion of the drainable porosity function is provided in appendix C, where we provide both explicit and approximate formulae for its implementation.

2.1.2. Overland flow

Turning now to the case where the soil is fully saturated, note that $H_g = L_z$, and then $H > L_z$. Then, as shown in appendix B, the surface depth evolves according to the following continuity equation:

$$\frac{\partial h_s}{\partial t} = \frac{\partial}{\partial x} (Q_g + Q_s) + r = \frac{\partial}{\partial x} \left(K_s L_z \frac{\partial h_s}{\partial x} + \frac{1}{n_s} \sqrt{S_x + \frac{\partial h_s}{\partial x}} h_s^k \right) + r(x, t). \quad (2.5)$$

In deriving the above, we have used the assumption that the overland (surface) flow is given by the empirical Manning's equation,

$$Q_s = \frac{1}{n_s} \sqrt{S_x + \frac{\partial h_s}{\partial x}} h_s^k, \quad (2.6)$$

where $k = 5/3$ and n_s is a Manning roughness coefficient, which depends on the hillslope surface type and is determined empirically (we use the typical value $n_s = 5.1 \cdot 10^{-2} \text{ ms}^{-1/3}$).

Now, we can combine eqs (2.3) and (2.5) into a single equation for H :

$$\frac{\partial H}{\partial t} = \begin{cases} f(x)^{-1} \left[\frac{\partial}{\partial x} (K_s H \frac{\partial H}{\partial x} + K_s H S_x) + r \right] & \text{if } H \leq L_z, \\ \frac{\partial}{\partial x} \left[K_s L_z \frac{\partial H}{\partial x} + \frac{1}{n_s} \sqrt{S_x + \frac{\partial H}{\partial x}} (H - L_z)^k \right] + r & \text{if } H > L_z. \end{cases} \quad (2.7)$$

We assume no-flow boundary conditions at the catchment boundary ($x = L_x$). At the location of the river ($x = 0$) we set constant $H_g = L_z$ (since the river water table is assumed to be located at the surface) and a (flat) free-surface condition for the overland flow, $\partial h_s / \partial x = 0$. In addition, in this work, we shall study the time evolution of the above system assuming that it is initially in equilibrium for a given mean rainfall $r_0 < r$, and then subjected to a rainfall r for $t > 0$. Therefore, for the initial condition, we shall take the steady-state of equation of (2.7) for a given mean rainfall r_0 . The boundary and initial conditions are summarised shortly in section 2.3.

2.2. Non-dimensional model

The above model can be nondimensionalised by taking $x = L_x x'$, $t = T_0 t'$, $H = L_z H'$ and $r = r_0 r'$. Here, $T_0 = L_x / (K_s S_x)$ is a characteristic timescale of the groundwater flow, chosen to balance temporal term and the $\partial_x (K_s H S_x)$ term.

Once non-dimensionalised, our governing equations (2.7) becomes (dropping primes)

$$\frac{\partial H}{\partial t} = \begin{cases} f(x)^{-1} \left[\frac{\partial}{\partial x} \left(\sigma H \frac{\partial H}{\partial x} + H \right) + \rho_0 r(x, t) \right] & \text{if } H \leq 1, \\ \frac{\partial}{\partial x} \left(\sigma \frac{\partial H}{\partial x} + \mu \sqrt{1 + \sigma \frac{\partial H}{\partial x}} (H - 1)^k \right) + \rho_0 r(x, t) & \text{if } H > 1, \end{cases} \quad (2.8a)$$

and the non-dimensional parameters σ , μ , and ρ_0 are introduced shortly in section 2.3. In this work, we assume that the rainfall is time- and spatially-independent, i.e. $r(x, t) = r = \text{constant}$. However, we shall discuss in §10 that our methodology can be applied in case of time-dependent rainfall.

In combination with the governing equations (2.8a) we have the following dimensionless boundaries conditions. First, at $x = 0$, dependent on whether surface flow is present,

$$0 = \begin{cases} H(0, t) - 1 & \text{if } H(0, t) \leq 1, \\ H_x(0, t) & \text{if } H(0, t) > 1, \end{cases} \quad (2.8b)$$

which expresses either that subsurface water matches river level if there is no surface water, or free-flow condition if surface water is present. At the right-hand edge, by definition of a catchment, there is zero flow:

$$q(1, t) = 0, \quad (2.8c)$$

where the flow, q , is defined as

$$q(x, t) = \begin{cases} H + \sigma H \frac{\partial H}{\partial x} & \text{if } H \leq 1, \\ 1 + \sigma \frac{\partial H}{\partial x} + \mu \sqrt{1 + \sigma \frac{\partial H}{\partial x}} (H - 1)^k & \text{if } H > 1. \end{cases} \quad (2.8d)$$

In this paper we refer to this model (2.8) as the *1D model*. The model will be supplemented with additional initial conditions to be discussed.

2.3. The non-dimensional parameters

Above, we have introduced three key dimensionless parameters, defined as

$$\sigma = \frac{L_z}{L_x S_x} = \frac{\text{soil depth}}{\text{elevation drop along the hillslope}}, \quad (2.9a)$$

$$\rho_0 = \frac{r_0 L_x}{L_z S_x K_s} = \frac{\text{precipitation rate}}{\text{groundwater flux}}, \quad (2.9b)$$

$$\mu = \frac{L_z^{k-1}}{S_x^{1/2} K_s n_s} = \frac{\text{overland flux}}{\text{groundwater flux}}. \quad (2.9c)$$

Note that $\sigma \rightarrow \infty$ as the hillslope becomes increasingly flat. The parameter ρ_0 represents the ratio of the total precipitation rate (given by rL_x in m^2s^{-1}) versus the maximum possible groundwater flow for fully saturated soil (given by $L_z S_x K_s$ in m^2s^{-1}). Finally, μ represents the relative strength of the overland flow affected by surface roughness. Based on typical scales of physical parameters used in the above equations provided in table 1 the typical scale of these dimensionless parameters is $\sigma \approx 10^{-2}$, $\mu \approx 10^7$ and $\rho_0 \approx 1.5$.

In fact, an additional key dimensionless parameter can be introduced in our later analysis of the $H > 1$ case of (2.8a). In the saturated zone, the dynamics are governed by the Péclet number,

$$\text{Pe} = \frac{\mu^{1/k}}{\sigma}, \quad (2.10)$$

which indicates the balance of convective and diffusive effects. Since typically μ is large, our work will primarily study $\text{Pe} \rightarrow \infty$ (equivalent to $\mu \rightarrow \infty$).

Kinematic approximation. As we discuss later in section 6.2, the height of surface water scales as $\mu^{-1/k}$ for $\mu \gg 1$. Therefore, in the $\mu \rightarrow \infty$ limit we can use so-called kinematic approximation,

$$\sqrt{1 + \sigma \frac{\partial H}{\partial x}} \sim 1.$$

which simplifies the saturated case ($H > 1$) of eqn (2.8a). Nevertheless, for now, we shall keep the first H -dependent term, since it plays an important role when investigating boundary effects.

PARAMETER	SYMBOL	MEAN VALUE	UNIT
Catchment width	L_x	700	m
Catchment depth	L_z	1	m
Hydraulic conductivity	K_s	10^{-3}	ms^{-1}
Precipitation rate	r	$1.59 \cdot 10^{-7}$	ms^{-1}
Hillslope gradient	S_x	0.075	—
Manning's roughness coefficient	n_s	1.19	$\text{sm}^{-1/3}$

Table 1: Typical values of physical parameters characterising hillslopes in low-productive aquifers in the UK. Parameters were extracted using methodology described in Part 1 (Morawiecki and Trinh 2022a).

3. Numerical methodology and typical dynamics

Recall that solutions are essentially characterised by the overland- and groundwater heights, and a quadruplet of parameters

$$H = H(x, t; \sigma, \mu, \rho_0, r), \quad (3.1)$$

as well as the constant $k = 5/3$ appearing in Manning's formula. These are solved by solving PDE (2.8a) subject to the boundary conditions (2.8) and (2.8c). In the typical configuration, the flow configurations transitions from overland $H > 1$ to groundwater $H \leq 1$, at a contact point $x = a(t)$, which is determined as part of the solution.

The model in (2.8a) was implemented in MatLAB using `ode15s` solver to find its steady state, and `pdepe` to solve the time-dependent problem. We divide the spatial and temporal domain via

$$x_i = \frac{i}{N_x} \quad \text{and} \quad t_j = \frac{j}{N_t} t_{\max}, \quad i, j = 1, 2, 3, \dots \quad (3.2)$$

where we typically use $N_x = 200$ and $N_t = 300$, checking whether increasing mesh size and time resolution does not significantly impact the obtained solution; if it does, the mesh is refined. The codes used to generate Figures in this work are available in a GitHub repository (Morawiecki 2022). All numerical results in the paper were obtained for values presented in table 1 unless stated otherwise.

3.1. Typical results for $\rho_0 < 1$ and $\rho_0 > 1$

The existence of the saturated zone in the initial steady state depends on whether the value of ρ_0 is higher or lower than 1, and each case will exhibit different transient behaviours. Typical solutions obtained in these two cases are shown in fig. 2.

First, consider fig. 2(a, b). In the case of $\rho_0 > 1$ we already have a saturated zone in the initial state. In a short timescale, the height of the surface water increases quickly until reaching a seemingly quasi-static state. Afterwards, the flow continues to increase as a result of the saturation front propagating uphill, but this process is characterised by much longer timescale and slower rate of flow rise. The difference between short- and long-time behaviour can also be seen on the produced hydrograph in fig. 3. In that figure, we have marked the initial fast transition as (A) and the subsequent slow transition as (B).

For $\rho_0 < 1$, we do not observe initial saturated zone, i.e. $H(x, t = 0) < 1$ for all x . For some time the groundwater table is rising, increasing groundwater flow reaching the river, until the groundwater depth gradient at $x = 0$ becomes 0. Then the saturated zone

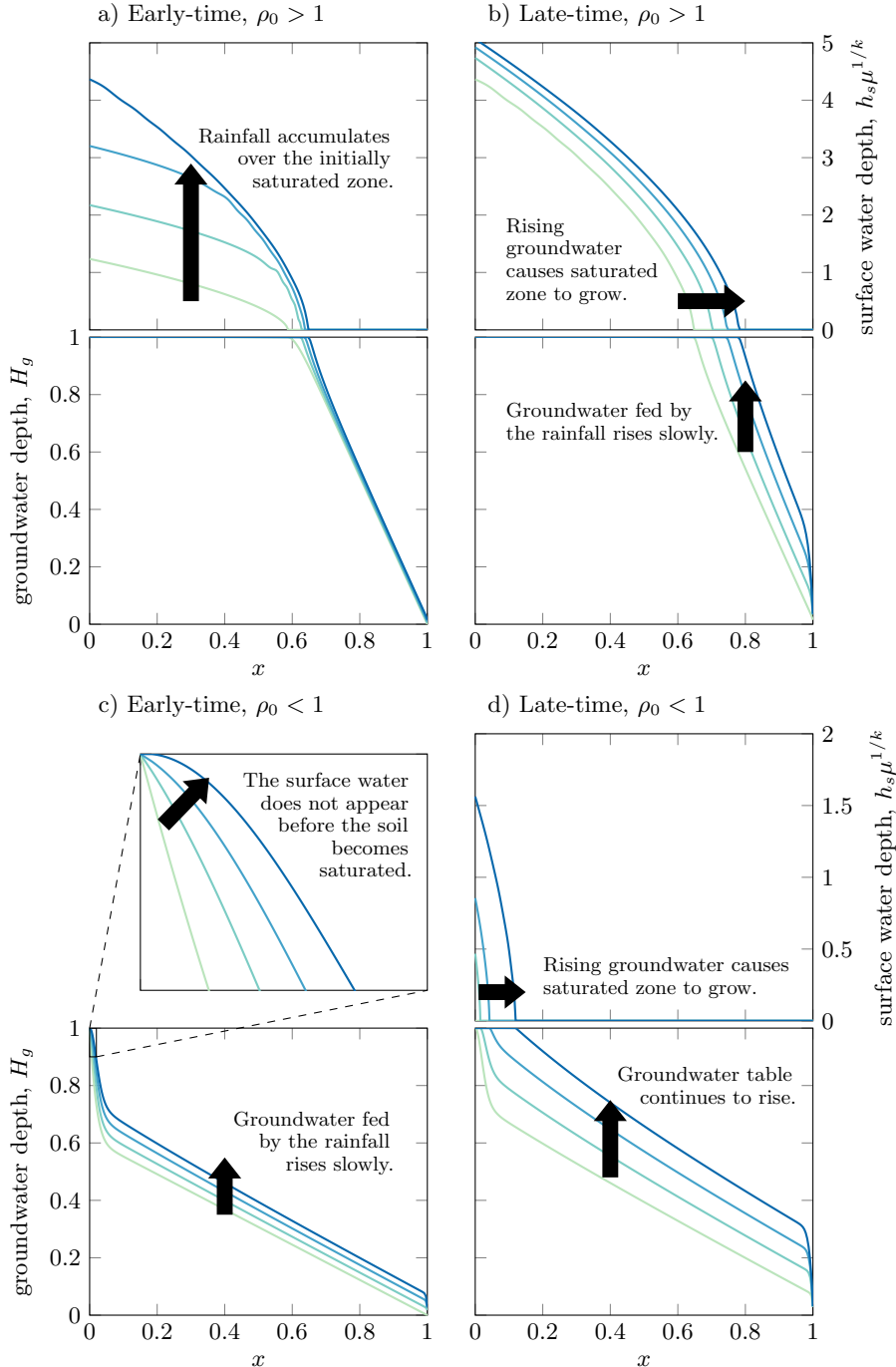


Figure 2: Schematic presenting early- and late-time dynamics for catchment with and without initially saturated zone (corresponding to $\rho_0 > 1$ and $\rho_0 \leq 1$ respectively).

starts to slowly form and propagate away from the channel, increasing the overland flow reaching the river.

However, in practice, in case of real-world catchments characterised by a thin layer of permeable soil (which is a base assumption behind the presented 1D model), the groundwater flow rate is highly limited. Therefore $\rho_0 > 1$ case is more prevalent, which is additionally confirmed by low BFI[†] values characterising low-productive catchments. This is why we focus this paper on discussing mathematical properties of each phase presented in fig. 3 only in the case of $\rho_0 > 1$.

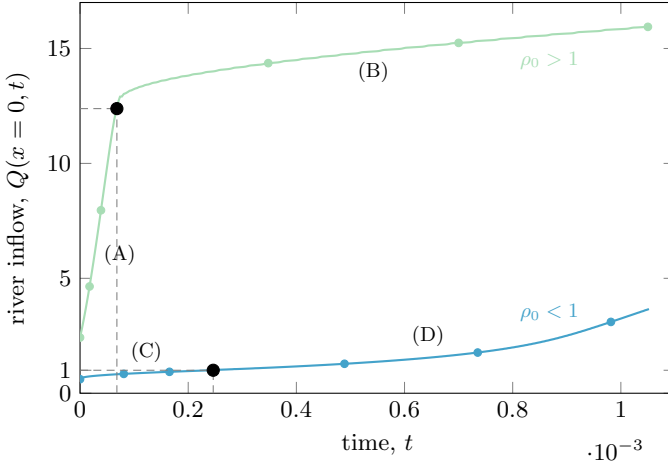


Figure 3: Schematic representation of hydrograph obtained for catchment with and without initially saturated zone (corresponding to $\rho_0 > 1$ and $\rho_0 \leq 1$ respectively). Points represent times, for which the profiles are shown in fig. 2, while letters A-D refer to corresponding phases from that figure.

In general, solution for PDE model (2.8a) can be found only numerically. However, by taking advantage of typical sizes of dimensionless parameters, the model can be further simplified. fig. 4 summarises dependence of hydrograph and steady states on model dimensionless parameters. Conclusions from this numerical experiment are the following:

- (i) **Parameter ρ_0** (typical value 2) has a significant impact on the initial steady state. As discussed in detail before, $\rho_0 < 1$ corresponds to hillslope with no initially saturated zone, and is characterised by different dynamics than $\rho_0 > 1$ case, in which we observe a fast rise of flow in early-time. In most of this paper, we will consider the latter case only.
- (ii) **Parameter ρ** (typical value ≈ 20) does not affect the initial steady state, but it does affect how quickly the flow is rising - higher ρ values, both create higher flow over saturated zone and lead to its faster growth. Values of ρ can vary significantly depending on the rainfall event considered.
- (iii) **Parameter σ** (typical value 10^{-2}) has a significant impact only on the solution in the unsaturated zone - in case of saturated zone, the term including σ is negligibly small comparing to μ term, however it will affect the speed with which the saturated zone is growing. Note that as $\sigma \rightarrow 0$ the initial groundwater shape becomes a

[†] BFI (Base Flow Index) describes the ratio between the base flow and total flow in the given catchment. High values refer to catchment dominated by the groundwater flow, while low values to catchments with significant overland flow component.

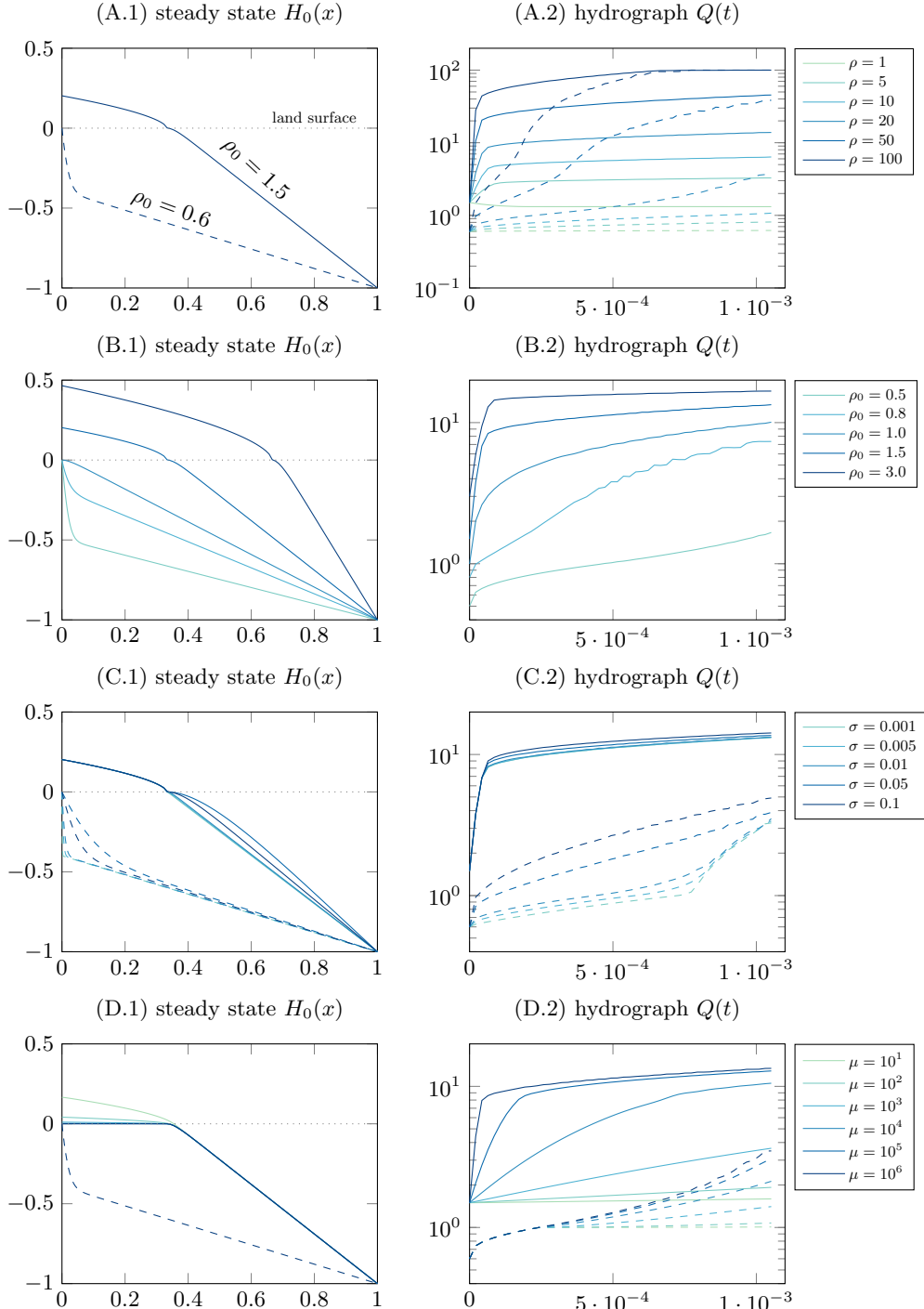


Figure 4: Impact of dimensionless parameters shown for the initial steady-state $H_0(x)$ vs x (insets left column) and for the hydrograph $Q(t)$ vs. t (insets right column). Insets (a, c, d) shows changing ρ_0 ; (b) for changing ρ ; (e, f) for changing σ ; and (g, h) for changing μ .

linear function (with possible small boundary layer at its left border). Even though this limit is not critical in our analysis, it may allow to approximate the initial groundwater shape, without a need to solve governing equations numerically.

(iv) **Parameter μ** (typical value 10^6) on the other hand, does not have significant impact on the unsaturated zone, however it has a huge impact on the height of the surface water. The higher μ values correspond to low surface water height, which in the limit $\mu \rightarrow \infty$ become negligible comparing to variation of groundwater depth. Also in this limit, the saturated zone size reaches a limiting value, $a_0 = 1 - \frac{1}{\rho_0}$ (see section 5). This limit is strongly supported by real-world data, and will allow us to derive the formula for a typical hydrograph.

4. The formulation of an asymptotic model for intense rain

In the previous section, we presented numerical simulations of the full PDE system (2.8) and showed that under some choice of parameters, the resultant hydrographs could be approximately classified according to the two behaviours shown in fig. 2. In particular, if the system was initiated with an initially-saturated zone, i.e. $\rho_0 > 1$, then in response to an intense rainfall, $r > 1$, the river inflow rapidly increases in time. Note that the duration of a standard intensive rainfall is shorter by few orders of magnitude than the typical timescale of the groundwater flow, which is

$$T_0 = \frac{L_x}{K_s S_x} \approx 1000 \text{ days.}$$

Our focus is to develop the short-time asymptotics in order to better understand this crucial response. Ultimately, we seek to produce an analytical scaling law for the flow at the river, $Q(t)$. Based on physical constraints, we are chiefly interested in the following asymptotic limits:

$$\begin{aligned} \text{small-time : } & t \ll 1, \\ \text{large overland-to-groundwater flow : } & \mu \gg 1 \text{ or } \text{Pe} \gg 1, \\ \text{intense rainfall : } & \rho = r\rho_0 \gg 1. \end{aligned} \quad (4.1)$$

To begin, let us reformulate the governing system in terms of a boundary-value-problem. We assume that there exists a single contact line located at $x = a(t)$ where $H(a(t), t) = 1$. This configuration is shown in fig. 1. From (2.8a) the evolution of these surfaces (assuming kinematic approximation) are governed by

$$\frac{\partial H}{\partial t} = \begin{cases} \frac{\partial}{\partial x} \left(\sigma \frac{\partial H}{\partial x} + \mu(H-1)^k \right) + \rho & \text{for } x \in [0, a(t)], \\ f(x)^{-1} \left[\frac{\partial}{\partial x} \left(\sigma H \frac{\partial H}{\partial x} + H \right) + \rho \right] & \text{for } x \in [a(t), 1]. \end{cases} \quad (4.2a)$$

$$\frac{\partial H}{\partial t} = \begin{cases} \frac{\partial}{\partial x} \left(\sigma \frac{\partial H}{\partial x} + \mu(H-1)^k \right) + \rho & \text{for } x \in [0, a(t)], \\ f(x)^{-1} \left[\frac{\partial}{\partial x} \left(\sigma H \frac{\partial H}{\partial x} + H \right) + \rho \right] & \text{for } x \in [a(t), 1]. \end{cases} \quad (4.2b)$$

Here for simplicity we have introduced $\rho = \rho_0 r$. Thus, we have a set of two time-dependent equations for H which are second-order in space, plus an additional contact-line position, $a(t)$, which can be regarded as an eigenvalue. Hence, five boundary conditions are required, in addition to the initial condition. Two boundary condition are required at $x = 0, 1$, and three matching conditions are required at the interface, $x = a(t)$. In total, these are

$$\partial_x H(0, t) = 0, \quad \partial_x H(1, t) = -\sigma^{-1}, \quad (4.3a-b)$$

$$H(a^-, t) = 1, \quad H(a^+, t) = 1, \quad \partial_x H(x = a^-, t) = \partial_x H(x = a^+, t). \quad (4.3c-e)$$

The boundary conditions follow from (2.8). The last interface condition is a consequence

of the continuity of flow given by (2.8d). Notice that a kinematic condition can be derived for the front position. Applying the chain rule to $H(a(t), t) = 1$, we have

$$\frac{\partial H}{\partial t} + \frac{\partial H}{\partial x} \frac{da}{dt} = 0 \quad \text{at } x = a(t). \quad (4.4)$$

We set initial condition given by the steady-state of eqs (4.2a)-(4.2b) for $r = 1$, which we write as $H_0(x; \rho_0)$. Thus H_0 satisfies

$$0 = \begin{cases} (\sigma H_0 H'_0 + H_0)' + \rho_0 & \text{for } x > a(0), \\ (\sigma H'_0 + \mu (H_0 - 1)^k)' + \rho_0 & \text{for } x \leq a(0), \end{cases} \quad (4.5)$$

where we have used primes ('') for differentiation in x .

We summarise the approach to come as follows.

- (i) First, in section 5, we study the initial state $H(x, 0) = H_0(x; r = 1)$, which is assumed to be the steady-state response to the rain input $r = 1$. This is a complicated coupled overland-groundwater problem, but we are able to develop analytical approximations in the limit of $\mu \rightarrow \infty$ or equivalently $\text{Pe} \rightarrow \infty$.
- (ii) Next, in section 6.1, we study the small-time response of the groundwater configuration and the propagation of the saturated zone. At the time $t = 0$, the rainfall is set to $r > 1$, which causes the groundwater to rise and the saturation zone to shift. Analytical approximations can be developed for the case of $\text{Pe} \rightarrow \infty$ and for large rainfalls, $r \rightarrow \infty$.
- (iii) Finally, in section 6.2, we develop an analytical approach for predicting the evolution of the overland flow, which leverages our analysis of the saturated zone propagation obtained in (ii). This turns out to be a wave propagation study using the method of characteristics.

5. Asymptotic analysis of the initial condition, H_0 , with $\text{Pe} \rightarrow \infty$

In our model, we assume that the system begins at the configuration that corresponds to the particular steady-state solution forced by the ‘typical’ rainfall, ρ_0 .

By integrating (4.5) and applying the boundary condition $q(1) = 0$, we obtain:

$$\rho_0(1 - x) = \begin{cases} H_0 + \sigma H_0 H'_0 & \text{for } x > a, \\ 1 + \sigma H'_0 + \mu(H_0 - 1)^k & \text{for } x \leq a. \end{cases} \quad (5.1a)$$

$$(5.1b)$$

The fact that the limit $\mu \rightarrow \infty$ involves the Péclet number, defined as $\text{Pe} = \mu^{1/k}/\sigma$ via (2.10) is not entirely obvious. Note that as $\mu \rightarrow \infty$, the dominant balance in the overland equation for $x \leq a$ indicates that $H_0 \sim 1$ in this limit. We re-scale $x = aX$ and $H_0 = \mu^{-1/k}g(X)$, obtaining, for $X \in [0, 1]$,

$$\frac{\text{Pe}^{-1}}{a} \frac{\partial g}{\partial X} + g^k = \rho_0(1 - aX) - 1, \quad (5.2)$$

$$g'(0) = 0 \quad \text{and} \quad g(1) = 0. \quad (5.3)$$

and so we see that the analysis of $\text{Pe} \rightarrow \infty$ involves the analysis of a singularly perturbed matched asymptotics problem.

Interestingly, the analysis for the asymptotic expansions of g and a is complicated because of boundary-layer phenomena. In appendix D, we develop these approximations in the limit of $\text{Pe} \rightarrow \infty$. There, we show that the contact line, $x = a$, and the gradient at

this point can be expanded into an asymptotic expansion,

$$a \sim a_0 + a_1 \text{Pe}^{-\beta} \quad \text{and} \quad H'_0(a) \sim \left[-\frac{\rho a_1}{\sigma} \right] \text{Pe}^{-\beta}, \quad (5.4)$$

where $\beta = k/(2k - 1)$ and the leading-order contact position is

$$a_0 = 1 - \frac{1}{\rho_0}. \quad (5.5)$$

Notice that increasing the rainfall rate, $\rho_0 \rightarrow \infty$, sends $a \rightarrow 1$ and overland water saturates the entire hillslope. In contrast, the limit $\rho_0 \rightarrow 1^+$ reduces saturated zone size to zero, as anticipated in section 3. The correction factor of a_1 in (5.4) can be calculated as an eigenvalue via the solution of a boundary-value problem [cf. eqn (D 7a)]. Finally, notice that as $\text{Pe}^{-1} \rightarrow 0$, the gradient at the transition between overland and groundwater flows, $H'_0(a) \rightarrow 0$.

As we shall show in section 6.1, in order to find the speed of saturated zone growth, we need to find the initial depth of the groundwater in the unsaturated zone first. We can do this by solving (5.1a), which can be rearranged to

$$\sigma \frac{dH_0}{dx} = \frac{\rho_0(1-x)}{H_0(x)} - 1 \quad \text{for } x \in [a, 1], \quad (5.6)$$

with a boundary condition $H_0(a) = 1$. This first-order nonlinear ODE does not have an explicit analytical solution – it can either be solved numerically or we can investigate its shape in different limits.

5.1. Analytical solution as $\sigma \rightarrow 0$

One quite useful limit is to consider $\sigma \rightarrow 0$ corresponding to the infinitely thin soil limit. In appendix E, we derive the outer asymptotic expansion for H_0 in terms of σ , (E 2), its inner expansion around $x = 0$ (E 4), and finally match them to form the following composite approximation for $H_0(x)$:

$$H_0(x) = \rho_0 \left(1 - x + \sigma - \sigma e^{-\frac{x-a_0}{\sigma}} \right), \quad \text{for } x \in [a_0, 1]. \quad (5.7)$$

As shown in fig. 5, this asymptotic solution provide a good approximation of the groundwater shape both for small σ values, and surprisingly also large σ values. In the latter case, H_0 becomes a linear function, which is also a limiting behaviour of our matched asymptotic solution (5.7).

6. Short-time asymptotics

This section relates to the asymptotic limits of $t \rightarrow 0$, $\mu \rightarrow \infty$, and $\rho = \rho_0 r \rightarrow \infty$ in (4.1).

6.1. Groundwater rise and propagation of the saturated zone

Having derived certain analytical properties of the steady-state configuration, $H_0(x; \rho_0)$ (used as an initial condition), we can now study the short-time behaviour of the system as the rain input is set to ρ . As argued at the start of section 4, this is a good approximation for typical rainfall of realistic duration.

As shown in appendix F, the outer solution for the unsaturated zone (4.2b) can be expanded into a regular series expansion in powers of the time:

$$H_{\text{outer}}(x, t) \sim H_0(x; \rho_0) + \left[\frac{\rho - \rho_0}{f(x)} \right] t + O(t^2). \quad (6.1)$$

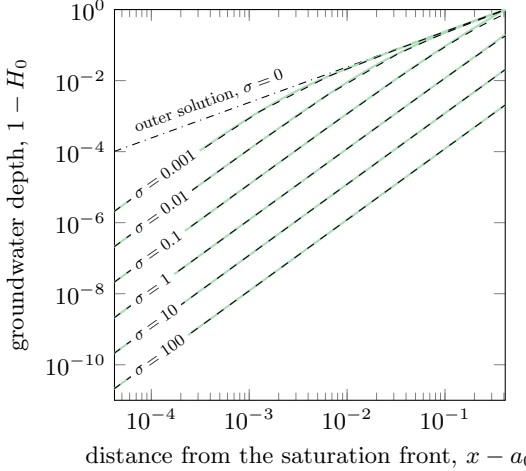


Figure 5: Comparison of groundwater depth given by (5.6) (full solution) to the matched asymptotic approximation given by (5.7).

The above approximation assumes that $x - a(t) = \mathcal{O}(1)$. The approximation (6.1) thus indicates that the groundwater rises in a fashion proportional to time and the difference between current and prior rain input; it correctly describes the shape of the groundwater except for a thin boundary layer at $x = a(t)$ of thickness of $\mathcal{O}(\sqrt{t/(\rho - \rho_0)})$ (see fig. 6a). Therefore, for intense rainfall, $\rho \gg 1$, we can neglect the effect of this boundary layer.

We may use the outer groundwater approximation, (6.1), in order to predict the motion of the contact line, $x = a(t)$. Setting $H_{\text{outer}} = 1$ this gives, in implicit form,

$$t \sim \frac{f(x = a(t))}{\rho - \rho_0} \left(1 - H_0(x = a(t))\right) \equiv \mathcal{T}(x = a(t)). \quad (6.2)$$

In order to calculate the above, we must solve two first-order ODEs: (5.6) for the height, $H_0(x)$, and (C2) for the head, $h_g(\hat{z})$, itself used in the calculation of $f(x)$. Alternatively, one can use the analytical approximations for $H_0(x)$ given by (5.7), and $f(x)$ given by (C6) or (C7). fig. 6b compares these approximations with the location of the saturation front computed from a full numerical solution of the 1D model. As we observe, neglecting boundary layer around $a(t)$ introduces a small error when estimating saturated zone size. Replacing the ODEs with analytical approximations for $f(x)$ and $H_0(x)$ also introduces an error, but it is significantly smaller.

6.2. Evolution of the overland flow

Now, knowing how the saturated zone propagates, we can develop a time-dependent solution for the overland flow. Our goal is to extract how the overland flow into the river, $Q_s(x = 0, t)$, evolves in time. Both the effects of increased rainfall, and the growing saturated zone are included.

6.2.1. Problem reduction under $\text{Pe} \rightarrow \infty$ limit

The equation for overland flow is given by (4.2a) with the initial condition satisfying steady state (5.1b). We re-scale according to

$$\eta = \mu^{1/k}(H - 1) \quad \text{and} \quad T = \mu^{1/k}t. \quad (6.3)$$

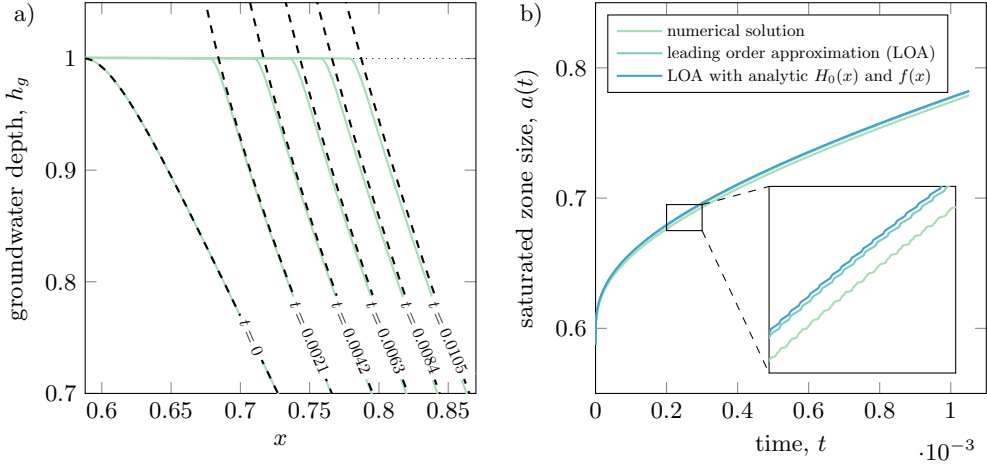


Figure 6: (a) Comparison of numerical solution of the groundwater shape with the outer solution developed in appendix F. Corresponding size of the saturated zone is presented in (b). Small region is zoomed to highlight differences between different approximations. The lines are not smooth, because of the $h(x)$ interpolation error.

Here $\eta = \eta(x, T)$ is a re-scaled surface water height $h_s = H - 1$. Then (4.2a) can be written as

$$\frac{\partial \eta}{\partial T} - k\eta^{k-1} \frac{\partial \eta}{\partial x} - \text{Pe}^{-1} \frac{\partial^2 \eta}{\partial x^2} = \rho, \quad (6.4)$$

and equation (5.1b), which provides the initial condition, H_0 , is

$$1 + \eta^k - \text{Pe}^{-1} \frac{d\eta}{dx} = \rho_0(1 - x). \quad (6.5)$$

where, as before, $\text{Pe}^{-1} = \sigma/\mu^{1/k}$. Note that the characteristic time of overland flow ($\mu^{-1/k}T_0 \approx 0.1$ day) is much shorter than the characteristic time describing groundwater zone ($T_0 \approx 1000$ days), and has a similar order of magnitude as a typical rainfall duration. As a result, a short-time approximation is not satisfactory to describe flow variation during a single rainfall event.

The solution for general times can be obtained by considering $\text{Pe} \rightarrow \infty$ limit, similarly as we did when analysing the steady state. This allows us to neglect the diffusion term everywhere except for a negligibly thin boundary layer around $x = a$.

In the limit $\text{Pe} \rightarrow \infty$, we expand $\eta = \eta_0 + \text{Pe}^{-1}\eta_1 + \dots$, and equation (6.4) becomes a first-order hyperbolic PDE:

$$\frac{\partial \eta_0}{\partial T} - \left[k\eta_0^{k-1} \right] \frac{\partial \eta_0}{\partial x} = \rho, \quad x \geq 0. \quad (6.6a)$$

For $0 \leq x \leq a(t)$, there is an initial condition given by

$$\eta_0(x, 0) = \rho_0^{1/k} (a_0 - x)^{1/k}, \quad (6.6b)$$

where we have used the fact shown in appendix D that $a_0 = 1 - 1/\rho_0$ [cf. (5.5)]. The above initial condition is defined along the whole initially saturated zone, $x \in [0, a_0]$. The necessary initial condition for $x > a(t)$ is discussed next.

6.2.2. Implicit solution using methods of characteristics

The system (6.6) can be solved using the method of characteristics (Lagrange–Charpit equations). The solution is given by characteristic curves (T, x, η_0) , now parameterised by (s, τ) , where τ is the characteristic curve parameter, and s parameterises the initial data. The characteristic equations are

$$\frac{dT}{d\tau} = 1, \quad \frac{dx}{d\tau} = -k\eta_0^{k-1}, \quad \frac{d\eta_0}{d\tau} = \rho. \quad (6.7a)$$

The initial conditions are specified along $\tau = 0$ according to two types of characteristics. One set of characteristics emerges from $T = 0$, at the location of the initial water shape, $H_0(x)$, valid for $x \in [0, a(t)]$. Another set of characteristics emerge from the propagating front, $x = a(t)$ —i.e. these represent the groundwater reaching the surface and hence initiating surface flow.

Parameterising the initial data by $x = s$, we have

$$(T(s, 0), x(s, 0), \eta_0(s, 0)) = \begin{cases} (0, s, H_0(s)), & s \in [0, a(t)], \\ (\mu^{1/k} \mathcal{T}(s), s, 0), & s \in [a(t), \infty). \end{cases} \quad (6.7b)$$

Above, the first condition will use the initial surface height, $H_0(s) = \rho_0^{1/k} (a_0 - s)^{1/k}$ given by (6.6b). The second condition is essentially specified along the moving front, $(T, x, \eta_0) = (T, a(t), 1)$, but we have written it in terms of the s -independent variable, and the rescaled function \mathcal{T} in (6.2). In summary, characteristic solution can be obtained via direct integration of (6.7), giving

$$\begin{aligned} T(s, \tau) &= T(s, 0) + \tau, \\ x(s, \tau) &= x(s, 0) - \rho^{-1} [\eta_0(s, 0) + \rho\tau]^k + \rho^{-1} [\eta_0(s, 0)]^k, \\ \eta_0(s, \tau) &= \eta_0(s, 0) + \rho\tau. \end{aligned} \quad (6.8)$$

We show an example of the characteristics and characteristic projections in fig. 7.

Once the solution has been determined, a key quantity is the surface water height at $x = 0$, since it determines the overland flow reaching the river. Let us denote this critical point along the characteristics by $(T, \eta_0) = (T^*, \eta^*)$. Setting $x(s, \tau) = 0$ in the above equations and eliminating τ from the second equation gives

$$\begin{pmatrix} T^* \\ \eta^* \end{pmatrix} = \begin{pmatrix} T(s, 0) + \frac{1}{\rho} (\eta^* - \eta_0(s, 0)) \\ \left(\rho x(s, 0) + (\eta_0(s, 0))^k \right)^{1/k} \end{pmatrix}. \quad (6.9)$$

Now we need to consider separately the characteristic curves starting from either the initially saturated zone, or the propagating interface between saturated and unsaturated zone—these are given by the different initial conditions in (6.7b).

In the first case, substituting the initial conditions to (6.9) gives

$$\begin{pmatrix} T^* \\ \eta^* \end{pmatrix} = \begin{pmatrix} \frac{1}{\rho} \left(\eta^* - \rho_0^{1/k} (a - s)^{1/k} \right) \\ (\rho s + \rho_0 (a - s))^{1/k} \end{pmatrix}. \quad (6.10)$$

By finding s from (6.10a) and substituting to (6.10b) we can find t^* as a function of η^* :

$$T^*(\eta^*) = \frac{1}{\rho} \left[\eta^* - \left(\frac{\rho_0}{\rho - \rho_0} \right)^{1/k} \left(\rho a_0 - (\eta^*)^k \right)^{1/k} \right], \quad (6.11)$$

This equation is satisfied for $\eta^* \in [(\rho_0 a_0)^{1/k}, (\rho a_0)^{1/k}]$, where the lower limit is the initial

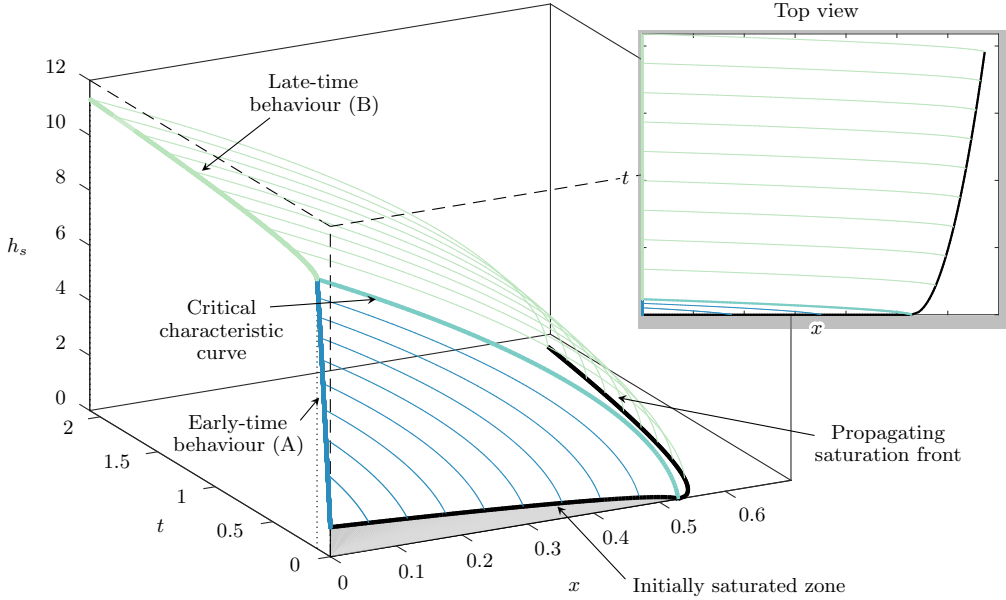


Figure 7: Characteristic curves given by (6.8) for parameters listed in table 1. Red lines represent curves originated from the initially saturated zone, and blue lines represent curves originated from the propagating front of the saturated zone.

height and upper limit is the height reached by the characteristic curve starting at $x_0 = a_0$. At the upper limit, the characteristic curve reaches the river ($x = 0$) at what we refer to as the *critical time*,

$$T_{\text{crit}} = \frac{1}{\rho} (\rho a_0)^{1/k}. \quad (6.12)$$

This critical saturation event is associated with the critical characteristic curve highlighted in fig. 7.

For those characteristics that emerge from the front, $x = a(t)$, we again substitute initial conditions (6.7b) to (6.9)

$$\begin{pmatrix} T^* \\ \eta^* \end{pmatrix} = \begin{pmatrix} \mu^{1/k} \mathcal{T}(s) + \frac{1}{\rho} \eta^* \\ (\rho s)^{1/k} \end{pmatrix}. \quad (6.13)$$

Eliminating s allow us to find t^* as a function of h_s^* :

$$T^*(\eta^*) = \mu^{1/k} \mathcal{T}\left(\frac{1}{\rho} (\eta^*)^k\right) + \frac{1}{\rho} \eta^*. \quad (6.14)$$

Combining equations (6.11) and (6.14) allows us to find the height of the surface water, at the river, $x = 0$, value for all time $T \geq 0$. It is given by solving the implicit equation

$$T^*(\eta^*) = \begin{cases} \frac{\eta^*}{\rho} - \frac{1}{\rho} \left(\frac{\rho_0}{\rho - \rho_0} \right)^{1/k} \left(\rho a_0 - (\eta^*)^k \right)^{1/k}, & \text{for } \eta^* \leq (\rho a_0)^{1/k}, \\ \frac{\eta^*}{\rho} + \mu^{1/k} \mathcal{T}\left(\frac{1}{\rho} (\eta^*)^k\right), & \text{for } \eta^* > (\rho a_0)^{1/k}. \end{cases} \quad (6.15)$$

Alternatively, we may relate the height of the surface water η^* to the overland component

of river inflow, which is represented by the last term in (2.8d), $Q_s^* = (\eta^*)^{1/k}$. This gives

$$t^*(Q_s^*) = \begin{cases} \frac{1}{\rho} (Q_s^*)^{1/k} - \frac{1}{\rho} \left(\frac{\rho_0}{\rho - \rho_0} \right)^{1/k} (\rho a_0 - Q_s^*)^{1/k}, & \text{for } Q_s^* \leq \rho a_0, \\ \frac{1}{\rho} (Q_s^*)^{1/k} + \mu^{1/k} \mathcal{T} \left(\frac{Q_s^*}{\rho} \right), & \text{for } Q_s^* > \rho a_0. \end{cases} \quad (6.16)$$

The above is one of the major results of this work, since it provides an analytic shape of a hydrograph $Q_s^*(t^*)$ expressed in an implicit form.

6.2.3. Approximating the hydrograph in an explicit form

We can obtain an approximated explicit form for $Q_s^*(t)$ function for $Q_s^* > \rho a_0$. In the limit $\mu \rightarrow \infty$ (equivalent to $\text{Pe} \rightarrow \infty$), we may expand about the value of Q_s^* at t_{crit} in (6.12), and write

$$Q_s^*(t^*) \sim \rho a \left(\mu^{-1/k} (t^* - t_{\text{crit}}) \right) \quad \text{for } t^* \geq t_{\text{crit}}, \quad (6.17)$$

where we have used $a(t) = \mathcal{T}^{-1}(t)$ from (6.2) to describe the propagation of the wetting front in time. Following approximation (5.7) and (C 7), it can be written explicitly as

$$a(t) = \underbrace{a_0}_{\text{term 1}} + \underbrace{s(t)}_{\text{term 2}} + \underbrace{\sigma \left[1 + W_0 \left(-e^{-1-s(t)/\sigma} \right) \right]}_{\text{term 3}}, \quad (6.18)$$

where

$$s(t) = At^{\frac{1}{n+1}} \quad \text{with} \quad A = \frac{1}{\rho_0} \left[\frac{n+1}{m} \frac{\rho - \rho_0}{\theta_s - \theta_r} \left(1 - \frac{r_0}{K_s} \right)^{-n} \alpha^{-n} \right]^{\frac{1}{n+1}}, \quad (6.19)$$

and $W_0(\cdot)$ is a Lambert W function. The first term in (6.17) corresponds to the flow over the initially saturated zone. The second and third terms represents growth of flow after reaching the critical point. The third term, in case of $\sigma \ll 1$, quickly grows from 0 asymptotically reaching σ as $t \rightarrow \infty$, while the second term is responsible for further growth of the river flow. Therefore, for thin hillslopes ($\sigma \ll 1$) the growth of river flow after passing the critical point scales proportionally to the ρA factor.

7. A numerical comparison between different approximations

7.1. Numerical setup

In Part 2 (Morawiecki and Trinh 2022b) we performed a numerical verification of the assumption of reducing the three-dimensional benchmark model to a two-dimensional model. We also performed a detailed sensitivity analysis, highlighting the dependencies of model parameters on the resultant peak flows. Here, we continue this analysis by comparing the hydrographs and peak flows between the five different approximations derived and discussed in this paper. The approximations are summarised in table 2 in an order from the most complex to the simplest.

Similar to the methodology presented in Parts 1 and 2, we assess performance of the above models in two ways. Firstly, we compare the hydrograph obtained using each model for standard values of parameters characterising UK catchments, as listed in table 3. Secondly, we run a sensitivity analysis by varying seven model parameters, one at a time, while keeping the others on their default values, and measuring the peak flow in the river after an intensive rainfall. In both numerical experiments, we consider a uniform rainfall over a duration of 24 hours.

APPROXIMATION		EQUATIONS/NOTES
2D surface-subsurface model		Richards/St Venant equations along a 2D hillslope, as discussed in (Morawiecki and Trinh 2022b)
1D surface-subsurface model		The 1D Boussinesq system (2.8), which assumes thin aspect ratio, $L_z \ll L_x$
Characteristics (numerically implicit)		Solution given by (6.16), where $H_0(x)$ and $f(x)$ functions are found numerically using 1D ODEs (5.6) and (C2). Assumes scenario $\rho_0 > 1$, early time $t \ll 1$, intense rainfall $\rho \gg 1$, and $\text{Pe} \gg 1$.
Characteristics (analytically implicit)		Solution given by (6.16), where functions $H_0(x)$ and $f(x)$ are approximated as (5.7) and (C6). Assumes in addition $\sigma \gg 1$, $H_0 \ll 1$.
Characteristics (analytically explicit)		Solution given by (6.17), $t_{\text{crit}} < t \ll 1$ (and assumptions listed before)
Critical flow		Flow estimated as $Q_{\text{crit}} = \rho a_0 + \rho_0(1-a_0)$, equal to river inflow reached at $t = t_{\text{crit}}$ (further discussion in section 8).

Table 2: Summary of approximations developed in this work.

PARAMETER	DEFAULT VALUE	PARAMETER RANGE	PARAMETER	VALUE
$K_s [\text{ms}^{-1}]$	$1 \cdot 10^{-5}$	$10^{-6} - 10^{-4}$	$L_y [\text{m}]$	18000
$L_x [\text{m}]$	$6.16 \cdot 10^2$	$10^2 - 10^3$	$w [\text{m}]$	5
$L_z [\text{m}]$	$6.84 \cdot 10^2$	$10^1 - 10^3$	$h_{\text{out}} [\text{m}]$	0.3
$S_x [-]$	$7.5 \cdot 10^{-2}$	$10^{-2} - 10^{-1}$	$\theta_s [-]$	0.488
$r [\text{ms}^{-1}]$	$2.36 \cdot 10^{-7}$	$3 \cdot 10^{-8} - 3 \cdot 10^{-6}$	$\theta_r [-]$	0
$r_0 [\text{ms}^{-1}]$	$2.95 \cdot 10^{-8}$	$10^{-9} - 10^{-7}$	$n [-]$	1.19
$n_s [\text{ms}^{-1/3}]$	$5.1 \cdot 10^{-2}$	$10^{-2} - 10^{-1}$		

Table 3: Default values and ranges of parameters used in order to perform the sensitivity analysis. The table on the right presents parameters not varied during sensitivity analysis.

7.2. Comparing the hydrograph

A comparison of the hydrograph obtained under the different approximations is presented in fig. 8. Firstly, we note that the 1D models formulated in this paper produce similar hydrographs as the 2D model from the previous part of our work; however, the 1D models very slightly underestimate the flow, and the solutions are not smooth around the critical point separating early-time and last-time growth.

Secondly, all approximated solutions of the 1D model produce consistent results for $t \leq t_{\text{crit}}$ (except for the explicit solution, which is valid only for $t > t_{\text{crit}}$). Also, the results are similar for $t > t_{\text{crit}}$, however inaccuracies related to different approximations start to become noticeable. For example, the implicit solution closely follows the 1D model solution, however, with the flow slightly shifted towards the higher values. This is caused by neglecting the boundary-layer characterising the groundwater shape around the critical point. As discussed in appendix F – this inaccuracy decreases as ρ increases. Replacing

numerical solutions for $f(x)$ and $H_0(x)$ with their analytic approximations does seem to have negligible impact on the model for typical sizes of catchment parameters.

Similarly, using approximation (6.17) for the explicit solution leads to the underestimation of groundwater rise rate, which slows down the growth of flow for higher t values. Also, the flow around $t = t_{\text{crit}}$ is slightly overestimated as a result of neglecting variation of $(Q_s^*)^{1/k}$ term appearing in the implicit solution (6.16). Despite these small inaccuracies, the explicit solution still seems to produce excellent qualitative and quantitative agreement. Moreover, due to its simple form, the explicit form allows us to directly understand the impact of various catchment properties on the expected peak flows.

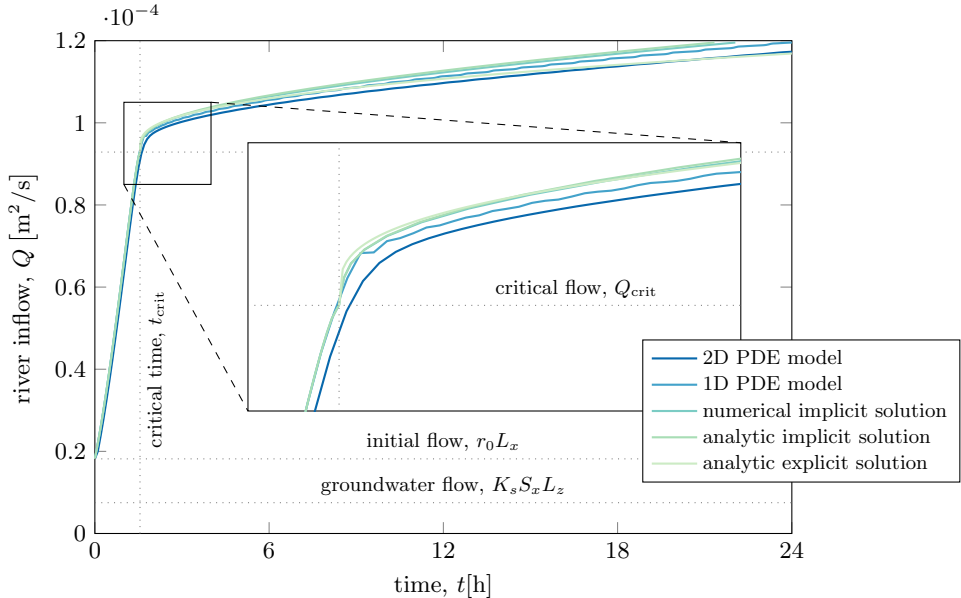


Figure 8: Hydrograph computed using approximations listed in table 2 for default values of parameters given in table 3. The graph area around the critical point is magnified.

7.3. Sensitivity analysis

Seven dimensional physical parameters were chosen for the sensitivity analysis: catchment width L_x , aquifer depth L_z , elevation gradient along hillslope S_x , hydraulic conductivity K_s , precipitations r and r_0 , and Manning's constant n_s . Each parameter is varied within the range of its typical values presented in table 3, while keeping other parameters constant. The results of the sensitivity analysis are presented in fig. 9.

We note that the nondimensional parameter that governs the initial saturation zone is given by $\rho_0 = rL_x/(K_s L_z S_x)$; therefore as the dimensional parameters are varied, the initial condition may not involve an initially saturated zone if $\rho_0 < 1$. Those relevant parameter ranges are marked by a dashed region in fig. 9. We observe that, as long as there exist an initially saturated zone, the analytical approximations of the hydrograph are largely accurate over the range of tested parameters.

As expected, the (total) peak flows reached are higher than those maximum levels set by the critical saturation flow, given by (8.1), since the latter only describes the flow reached during the early-time phase. Nevertheless, in most of the parameter values, the

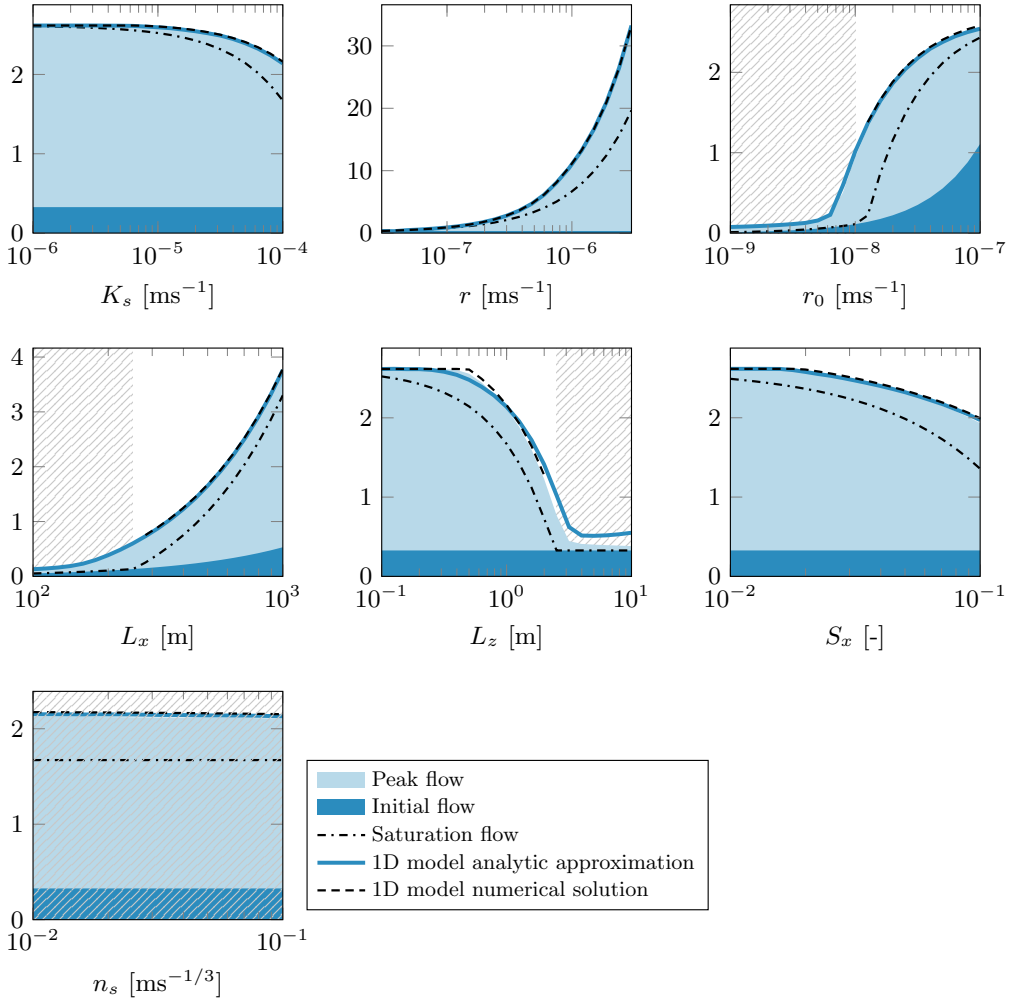


Figure 9: Sensitivity analysis results showing dependence between peak flow reached after an intensive rainfall and seven model parameters. The predictions conducted using four models of varying complexity are presented. The dashed region represents the parameter range, for which there is no initially saturated zone ($\rho_0 < 1$).

critical flow curve provides a good approximation of the peak flows. In Part 2 of our work, based purely on the 3D and 2D simulations, we had arrived at the same conclusion.

The cases where the critical saturation value highly underestimates the peak flow is around $\rho_0 = 1$. In cases where there is a very small initially-saturated zone (ρ_0 slightly larger than 1) we observe that the saturated zone can grow significantly during rainfall; this is not captured by the time-independent estimate (8.1). The same argument applies for the simulations with no initially saturated zone, but where the groundwater is located close enough to the surface (ρ_0 slightly less than 1) to allow for fast growth of the saturation zone. We imagine that these cases will involve asymptotic analysis in the distinguished limits of $\rho_0 \rightarrow 1$ simultaneous to $t \rightarrow 0$.

8. Summary of key hydrograph features

In fig. 8 in the previous section we showed a typical shape of hydrograph given by the 1D model. Here we summarise the main features of the hydrograph and its importance in the benchmarking.

As discussed before, two different phases are visible: (phase 1) an early-time fast rise caused by water accumulating over an initially saturated zone, and (phase 2) a late-time slow rise caused by a growing saturated zone. Analytic approximations presented in section 6.2 show that the transition between these two phases corresponds to the moment when the characteristic curve starting from the further-most point of the initially saturated zone reaches the river ($x = 0$). This allowed us to estimate dimensionless critical time t_{crit} (6.12). The corresponding (dimensionless) critical flow is $Q_{\text{crit}} = 1 + \rho a_0$, where the first term represents the groundwater flow, and the second term represents the overland flow generated over the initially saturated zone. In the dimensional units, the critical flow is

$$Q_{\text{crit}} = \underbrace{K_s S_x L_z}_{\text{groundwater flow}} + r L_x \underbrace{\left(1 - \frac{K_s S_x L_z}{r_0 L_x}\right)}_{\text{overland flow}}, \quad (8.1)$$

which occurs at the critical time,

$$t_{\text{crit}} = \frac{L_z}{r} \left[\frac{S_x^{1/2} K_s n}{L_z^{k-1}} \left(\frac{L_x r}{K_s S_x L_z} - \frac{r}{r_0} \right) \right]^{1/k}. \quad (8.2)$$

Following the above event, further growth is slow, which is a result of the difference of $\mu^{1/k} \approx 10^4$ factor between the characteristic timescale of overland flow (responsible for phase 1) and groundwater flow (responsible for phase 2).

We highlight a few additional features:

- (i) Typically the groundwater component of Q_{crit} (8.1) is much smaller than the overland component, especially for intensive rainfalls. Therefore, the critical point reached during extreme rainfalls can be approximated by

$$Q_{\text{crit}} \approx r L_x \left(1 - \frac{K_s S_x L_z}{r_0 L_x} \right) \quad (8.3)$$

Since the consecutive river flow rise is slow, the above estimate can be used as an approximation of peak flow reached, assuming that rainfall is long enough to reach the critical time, t_{crit} .

- (ii) Under this approximation, the critical point can be therefore represented a function of three parameters: rainfall intensity, catchment area (since the flow scales proportionally to both hillslope width L_x and catchment length L_y), and the $K_s S_x L_z / (r_0 L_x)$ factor, which is equal to fraction of groundwater flow $K_s S_x L_z$ to mean total flow $r_0 L_x$. This last parameter can be related to what is often referred-to as the Base Flow Index, BFI (Gustard et al. 1992, Sec. 3.1.2).
- (iii) The three parameters listed in (ii) are also used as catchment descriptors in statistical methods for estimating peak flows, which is recommended for use in the UK in Flood Estimation Handbook (FEH, Robson and Reed 1999). There are a few differences. The first difference is that FEH method uses mean rainfall (SAAR) instead of peak rainfall; however the two measures are linearly related, as shown in Part 1. The second difference is that FEH uses the additional descriptor of Flood Attenuation by Reservoirs and Lakes (FARL); however, this measure is

always equal to 1 for catchments which do not include lakes and reservoirs, like the one we consider in our benchmark scenario.

The connection between our simple scaling laws, shown above, and derived analytically, with statistical models that are formulated in a completely different fashion is intriguing. This subject forms ongoing work by the present authors.

9. Conclusions

The primary aim of our work has been to develop and analyse a rigorous benchmark scenario for coupled surface/subsurface flows in a prototypical catchment. We have done this by firstly characterising the typical parameter scales according to the available data on UK catchments (Part 1), formulating and computing the 3D model and its reduction (Part 2), and finally applying methods in asymptotic analysis to a reduced model valid for the catchments dominated by overland dynamics (Part 3).

In this last work, our analysis yields valuable scaling laws for the peak flows (section 8), which precisely quantify the observed separation of time-scales observed in the hydrographs following an intense period of rain. In particular, we find that the early-time behaviour is governed by rainfall accumulation over a pre-existing saturation zone, following by a slower flow rise in late-time; this latter stage is limited by the speed with which the rising groundwater increases the size of the saturated zone. All approximation are in good agreement with hydrographs produced by the more complete 1D and 2D models, and allow accurate prediction of river peak flows over a wide range of catchment parameters (as long as underlying assumptions are satisfied).

10. Discussion

Our investigations in these three parts have been limited to fairly elementary scenarios and geometries. However, our final results involving the derivation of analytical/asymptotic scaling laws with a clear underlying structure may serve as a valuable benchmark for other hillslope or catchment models. Currently, we have observed that the benchmarking of catchment models has been limited to quantitative numerical comparisons, either with real-world observations, or with the numerical output of other schemes (e.g. [Maxwell et al. 2014](#)). While such studies allow practitioners to evaluate the given model's performance in specific conditions, it does not necessarily allow one to draw general conclusions about each model's limit of applicability. As it concerns data-oriented models, we have no guarantee that the model will still perform well if applied in situations not captured in the training or validation data.

Deriving asymptotic estimates for the hydrograph opens another possibility: *models can be compared at a more fundamental level*. Thus for instance, we may check if the flows produced by various models scale with the different catchment properties in the expected fashion (and under the conditions we have specified). As a particular example, statistical models used for flood estimation require the selection of a set of catchment descriptors, and then often use regression formulae in order to relate such descriptors to the desired river flow properties ([Kjeldsen et al. 2008](#)). Comparing such models with our benchmark solutions may allow us to detect those situations or limits where predictions diverge; this exercise can also shed light on how those statistical regression formulae can be extended beyond their current limit of applicability.

Similarly, we may compare the analytical solutions developed in our physical benchmark model with those flow hydrographs generated via conceptual rainfall-runoff models. This

would allow us to assess intrinsic simplifying assumptions found in conceptual models, and furthermore their parameters can be more directly linked with physical parameters in the benchmark. In turn, this analysis may shed light on how conceptual models can be tuned to better approximate behaviour of complex-real world systems. Work on these questions is ongoing (Morawiecki and Trinh 2022c,d).

Lastly, we mention that an important further line of enquiry is the generalisation of the analysis we have presented to situations that are more general and representative (although this does interfere slightly with the need for simplicity in benchmarking scenarios). Such extensions can involve the analysis of non-uniform rainfall, varying initial conditions to study response to extended periods of drought. In the latter case, analytical approximations of the drying process could be used to assess the assumptions of the conceptual rainfall-runoff models, especially since dry periods are sometimes used for a preliminary parameter calibration (Lamb 1999). Finally, we highlight the importance of multi-porosity regions in hydrological modeling; this leads to effects such as flows through macropores that are not described by our models (Beven and Germann 2013).

Acknowledgements. We thank Sean Longfield (Environmental Agency) for useful discussions, and for motivating this work via the 7th Integrative Think Tank hosted by the Statistical and Applied Mathematics CDT at Bath (SAMBa). We also thank Thomas Kjeldsen, Tristan Pryer, Keith Beven and Simon Dadson for insightful discussions. Piotr Morawiecki is supported by a scholarship from the EPSRC Centre for Doctoral Training in Statistical Applied Mathematics at Bath (SAMBa), under the project EP/S022945/1.

REFERENCES

M. G. Anderson and S. Brooks. *Advances in hillslope processes*, volume 1. Wiley, 1996.

M. S. Bartlett and A. Porporato. A class of exact solutions of the Boussinesq equation for horizontal and sloping aquifers. *Water Resour. Res.*, 54(2):767–778, 2018.

J. C. Bathurst, J. Ewen, G. Parkin, P. E. O’Connell, and J. D. Cooper. Validation of catchment models for predicting land-use and climate change impacts. 3. Blind validation for internal and outlet responses. *J. Hydrol.*, 287(1-4):74–94, 2004.

J. Bear and A. Verruijt. *Modeling groundwater flow and pollution*, volume 2. Springer Science & Business Media, 1987.

K. Beven. On hypothesis testing in hydrology: Why falsification of models is still a really good idea. *Wiley Interdiscip. Rev.: Water*, 5(3):e1278, 2018.

K. Beven and P. Germann. Macropores and water flow in soils revisited. *Water Resour. Res.*, 49(6):3071–3092, 2013.

J. Boussinesq. *Essai sur la théorie des eaux courantes*. Imprimerie nationale, 1877.

J.-G. Caputo and Y. A. Stepanyants. Front solutions of Richards’ equation. *Transp. Porous Media*, 74(1):1–20, 2008.

F. J. Cook, J. H. Knight, and R. A. Wooding. Steady groundwater flow to drains on a sloping bed: Comparison of solutions based on Boussinesq equation and Richards equation. *Transp. Porous Media*, 77(2):357–372, 2009.

J. Dupuit. *Études théoriques et pratiques sur le mouvement des eaux dans les canaux découverts et à travers les terrains perméables: avec des considérations relatives au régime des grandes eaux, au débouché à leur donner, et à la marche des alluvions dans les rivières à fond mobile*. Dunod, 1863.

P. Forchheimer. *Hydraulik*. BG Teubner, 1914.

R. B. Grayson, I. D. Moore, and T. A. McMahon. Physically based hydrologic modeling: 2. Is the concept realistic? *Water Resour. Res.*, 28(10):2659–2666, 1992.

A. Gustard, A. Bullock, and J. M. Dixon. *Low flow estimation in the United Kingdom*. Institute of Hydrology, 1992.

V. Hálek and J. Švec. *Groundwater hydraulics*. Elsevier, 2011.

F. M. Henderson and R. A. Wooding. Overland flow and groundwater flow from a steady rainfall of finite duration. *J. Geophys. Res.*, 69(8):1531–1540, 1964.

M. J. Kirkby. Infiltration, throughflow, and overland flow. In *Intro. Fluv. Proc.*, pages 85–97. Routledge, 2019.

M. J. Kirkby and K. J. Beven. A physically based, variable contributing area model of basin hydrology. *Hydrol. Sci. J.*, 24(1):43–69, 1979.

T. R. Kjeldsen, D. A. Jones, and A. C. Bayliss. *Improving the FEH statistical procedures for flood frequency estimation*. Environment Agency, 2008.

R. Lamb. Calibration of a conceptual rainfall-runoff model for flood frequency estimation by continuous simulation. *Water Resour. Res.*, 35(10):3103–3114, 1999.

I. MacDonald, M. J. Baines, N. K. Nichols, and P. G. Samuels. Comparison of some steady state Saint-Venant solvers for some test problems with analytic solutions. *Numerical analysis report*, 2:95, 1995.

R. M. Maxwell, M. Putti, S. Meyerhoff, J.-O. Delfs, I. M. Ferguson, V. Ivanov, J. Kim, O. Kolditz, S. J. Kollet, M. Kumar, et al. Surface-subsurface model intercomparison: A first set of benchmark results to diagnose integrated hydrology and feedbacks. *Water Resour. Res.*, 50(2):1531–1549, 2014.

R. J. Moore, V. A. Bell, S. J. Cole, and D. A. Jones. Rainfall-runoff and other modelling for ungauged/low-benefit locations. Technical report, Research Contractor: CEH Wallingford, Environment Agency, Bristol, UK, 2007.

P. Morawiecki. GitHub repository for 3D, 2D and 1D benchmark catchment models. <https://github.com/Piotr-Morawiecki/benchmark-catchment-model>, 2022. Accessed: 2022-10-28.

P. W. Morawiecki and P. H. Trinh. On the development and analysis of coupled surface-subsurface models of catchments. Part 1. Parameter estimation and sensitivity analysis of catchment properties. *T.B.C.*, 2022a.

P. W. Morawiecki and P. H. Trinh. On the development and analysis of coupled surface-subsurface models of catchments. Part 2. A three-dimensional benchmark model and its properties. *T.B.C.*, 2022b.

P. W. Morawiecki and P. H. Trinh. The application of analytical physical benchmarks to assess conceptual rainfall-runoff models. *In preparation*, 2022c.

P. W. Morawiecki and P. H. Trinh. The application of analytical physical benchmarks to improve flood estimation methods. *In preparation*, 2022d.

C. Paniconi, P. A. Troch, E. E. Van Loon, and A. G. J. Hilberts. Hillslope-storage Boussinesq model for subsurface flow and variable source areas along complex hillslopes: 2. Intercomparison with a three-dimensional Richards equation model. *Water Resour. Res.*, 39(11), 2003.

G. Parkin, G. O'donnell, J. Ewen, J. C. Bathurst, P. E. O'Connell, and J. Lavabre. Validation of catchment models for predicting land-use and climate change impacts. 2. Case study for a Mediterranean catchment. *J. Hydrol.*, 175(1-4):595–613, 1996.

J.-Y. Parlange, C. W. Rose, and G. Sander. Kinematic flow approximation of runoff on a plane: An exact analytical solution. *J. Hydrol.*, 52(1-2):171–176, 1981.

P. Polubarnova-Kochina and R. D. Wiest. *Theory of groundwater movement*. Princeton University, 1962.

A. J. Robson and D. W. Reed. Statistical procedures for flood frequency estimation. Volume 3 of the Flood Estimation Handbook. Technical report, Centre for Ecology & Hydrology, 1999.

E. Shaw, K. Beven, N. Chappell, and R. Lamb. *Hydrology in practice*. CRC press, 3 edition, 2010.

M. Sulis, S. B. Meyerhoff, C. Paniconi, R. M. Maxwell, M. Putti, and S. J. Kollet. A comparison of two physics-based numerical models for simulating surface water–groundwater interactions. *Adv. Water Resour.*, 33(4):456–467, 2010.

W. Tao, Q. Wang, and H. Lin. An approximate analytical solution for describing surface runoff and sediment transport over hillslope. *J. Hydrol.*, 558:496–508, 2018.

F. T. Tracy. Clean two-and three-dimensional analytical solutions of Richards' equation for testing numerical solvers. *Water Resour. Res.*, 42(8), 2006.

P. A. Troch, C. Paniconi, and E. Emiel van Loon. Hillslope-storage Boussinesq model for

subsurface flow and variable source areas along complex hillslopes: 1. Formulation and characteristic response. *Water Resour. Res.*, 39(11), 2003.

P. A. Troch, A. Berne, P. Bogaart, C. Harman, A. G. J. Hilberts, S. W. Lyon, C. Paniconi, V. R. N. Pauwels, D. E. Rupp, J. S. Selker, et al. The importance of hydraulic groundwater theory in catchment hydrology: The legacy of Wilfried Brutsaert and Jean-Yves Parlange. *Water Resour. Res.*, 49(9):5099–5116, 2013.

A. W. Warrick, D. O. Lomen, and A. Islas. An analytical solution to Richards' equation for a draining soil profile. *Water Resour. Res.*, 26(2):253–258, 1990.

R. A. Wooding and T. G. Chapman. Groundwater flow over a sloping impermeable layer: 1. Application of the Dupuit-Forchheimer assumption. *J. Geophys. Res.*, 71(12):2895–2902, 1966.

D. A. Woolhiser and J. A. Liggett. Unsteady, one-dimensional flow over a plane—The rising hydrograph. *Water Resour. Res.*, 3(3):753–771, 1967.

Appendix A. List of symbols

For ease of reference, we provide a list of symbols in table 4.

group	symbol	description
coordinates	x	spatial coordinate along the hillslope
	t	time
variables	H_g	groundwater depth
	h_s	surface water depth
	H	total depth ($H_g + h_s$)
	H_0	initial value of total depth
	Q_g	groundwater flux
	Q_s	overland flux
catchment	L_z	soil depth
properties	S_x	slope along the hillslope
	r	rainfall intensity
	K_s	hydraulic conductivity
	f	mean drainable porosity (typically function of x)
	θ_s, θ_r	saturated and residual water content
	α, n, m	Maulem Van Genuchten model parameters
	T_0	characteristic timescale of groundwater flow
	n_s	Manning roughness coefficient
	k	exponent form the Manning's law (typically $k = 5/3$)
dimensionless	σ	soil depth to elevation drop ratio
constants	μ	overland to groundwater flux ratio
	ρ	precipitation rate to groundwater flux ratio
	ρ_0	mean precipitation rate to groundwater flux ratio
	$\Delta\rho$	difference between ρ and ρ_0
	Pe	Péclet number for the overland flow
	a	saturated fraction of the hillslope
	a_0	leading order approximation of a for $Pe \rightarrow \infty$
characteristic	T	rescaled time for the overland flow model
curves	η	rescaled surface water height for the overland flow model
	τ	characteristic curve parameter
	s	parameter describing initial data
	T^*, η^*, Q_s^*	value of time, surface water height and surface flow, when characteristic curve reaches $x = 0$
	t_{crit}	critical time
	Q_{crit}	critical point
simulation	N_x	spatial mesh resolution
parameters	N_t	number of time steps

Table 4: List of symbols

Appendix B. Relation between the 1D Boussinesq equation and the 2D Richards equation

In this appendix, we provide additional details on the derivation of the 1D model presented in this paper, in connection with the physical models presented in Part 2. This relates to governing equations (2.3) and (2.5) starting from the two-dimensional Richards equation given in eqn (A5) from Part 2 (Morawiecki and Trinh 2022b). Some parts of the following are classical, and relate to the derivation of the Boussinesq approximation [cf. Bear and Verruijt (1987) for details]; our new contribution is to consider the influence of the overland flow in the saturated zones on the Boussinesq approximation, and to couple this latter equation with its standard formulation for the unsaturated zone.

In this study, we will assume that hillslope flow is predominantly two-dimensional in xz -cross section; this reduction from three dimensions to two dimensions is discussed in detail in Part 2. In addition, we consider the small aspect ratio limit, $L_z \ll L_x$, and hence $\beta_{zx} = L_z/L_x \rightarrow 0$. In the groundwater region, the leading-order flow then satisfies

$$\frac{d\theta}{dh} \Big|_{h=h'_g} \frac{\partial h'_g}{\partial t} = \frac{\partial}{\partial \hat{z}} \left[K_r(h'_g) \left(\frac{\partial h'_g}{\partial \hat{z}} + 1 \right) \right], \quad 0 < \hat{z} < 1, \quad (\text{B1})$$

with $\hat{z} = 0$ corresponding to the bottom of the aquifer and $\hat{z} = 1$ corresponding to the top surface. Note that for $\hat{z} < H$, Richards equation becomes much simpler, since for saturated soil we have $\frac{d\theta}{dh} = 0$ and $K_r(h) = 1$. Solving (B1) and imposing the no-flow boundary condition at the bottom of the aquifer $\hat{z} = 0$, we have

$$h'_g(\hat{x}, \hat{z}, t) = H'(\hat{x}, t) - \hat{z}, \quad 0 < \hat{z} < H'(\hat{x}, t), \quad (\text{B2})$$

which corresponds to a hydrostatic vertical profile of pressure. Note that based on the above solution, for regions of completely saturated soil, the two-dimensional function $h'_g(\hat{x}, \hat{z}, t)$ can be replaced by the one-dimensional indicator, $H'(\hat{x}, t)$. The curve $\hat{z} = H'(\hat{x}, t) \in (0, 1]$ corresponds to the groundwater table, which separates between saturated (where $h'_g > 0$) and unsaturated (where $h'_g < 0$) regions, if both coexist.

We assume that the system is configured as shown in fig. 10. Thus it is divided into a Region (B, fully saturated case) where $0 \leq \hat{x} \leq a(t)$ and the ground is entirely saturated, with $H = 1$. Similarly we have Region (A, unsaturated case), for $\hat{x} > a(t)$, where $H < 1$ and there is an unsaturated column where $H < \hat{z} < 1$.

For ease of interpretation, we shall return, for the next few subsections to dimensional quantities [related to the governing equation (2.7)]. In addition, it is more convenient to use Richards equation expressed in the Cartesian coordinates (x, z) . In this coordinate system, (B2) becomes

$$h_g(x, z, t) = S_x x + H(x, t) - z, \quad \text{for } x \in [0, L_x], z \in [0, L_z] \quad (\text{B3})$$

under $L_z \hat{z} = z - S_x x$, $H = L_z H'$ and $h_g = L_z h'_g$. From Darcy's law as $\mathbf{q} = K_s \nabla (h_g + z)$. After substituting (B3), we obtain the leading term of horizontal flow:

$$q_x = -K_s \frac{\partial}{\partial x} (h_g + z) = -K_s \left(S_x + \frac{\partial H}{\partial x} \right). \quad (\text{B4})$$

Note that the above point flux is independent on z . Multiplying by H , we thus see that the total (unsigned) flow along the hillslope is then given by

$$Q_g = H|q_x| = K_s H \frac{\partial H}{\partial x} + K_s H S_x \quad (\text{B5})$$

Next we shall consider unsaturated (Region A) and saturated (Region B) zones separately, since the latter requires adding an overland flow component.

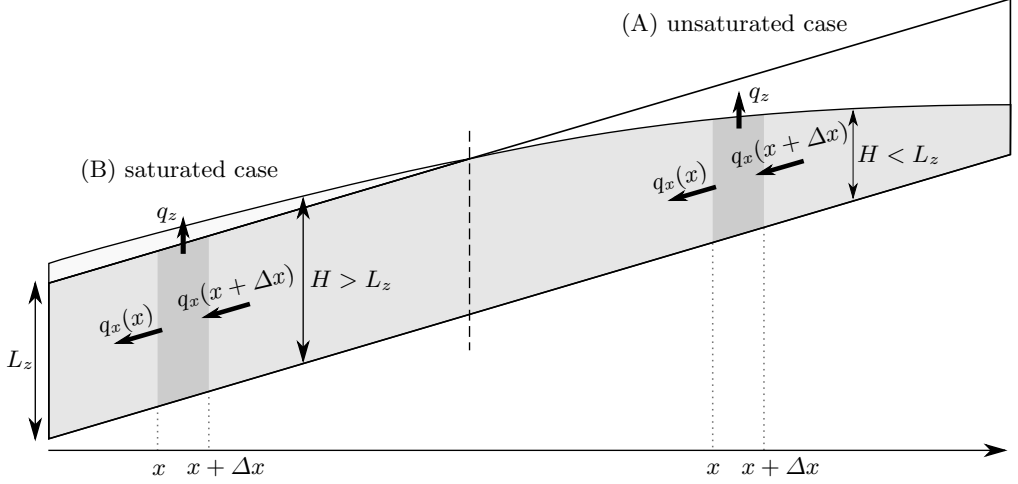


Figure 10: Control volume in (A) the unsaturated zone, and (B) the unsaturated zone. One-way arrows represent flow in and out of the control volumes.

B.1. (Region A) Governing equation for the unsaturated zone, $H < 1$

Let us consider Region A, where there is a layer of unsaturated soil. Recall the pressure h_g is zero at the free-surface of the groundwater, where $z = S_x x + H_g(x, t)$. This allows us to set the integration constant H appearing in (B3) to $H(x, t) = H_g(x, t)$.

We consider the control volume, V , within the column horizontally bounded by $[x, x + \Delta x]$, and shown in fig. 10. By conservation and the divergence theorem, it is argued that the total flux integral around the boundary, ∂V , is zero, and hence

$$0 = \oint_{\partial V} \nabla(h + z) \cdot \mathbf{n} \, dl \\ = -H(x)q_x(x) + H(x + \Delta x)q_x(x + \Delta x) + \int_x^{x + \Delta x} q_z \Big|_{z=S_x x + H(x)} \, dx. \quad (B6)$$

where from the argument following (A1), we have used that Richards equation in the fully saturated groundwater region reduces to $\nabla \cdot \mathbf{q} = K_s \nabla^2(h + z) = 0$. Thus, in the limit $\Delta x \rightarrow 0$, we then have an approximation for the vertical flux at the top of the saturated zone:

$$q_z \Big|_{z=S_x x + H(x)} = -\frac{\partial}{\partial x} (Hq_x) = K_s \frac{\partial}{\partial x} \left(HS_x + H \frac{\partial H}{\partial x} \right), \quad (B7)$$

where we have used q_x derived in (B4).

In order to derive an equation for $H(x, t)$, we apply mass conservation characterising the exchange of vertical flow between the unsaturated column $0 < z < H$ and the saturated column $H < z < L_z$. Let \mathcal{V} denote the groundwater volume per unit area. We define the *drainable porosity* as,

$$f(x, t) \equiv \frac{d\mathcal{V}}{dH}. \quad (B8)$$

In essence, $f(x, t)$, describes, for a given change in the height, H , the corresponding change in the groundwater volume, \mathcal{V} . This quantity is further discussed in appendix C.

Then taking into account the groundwater recharge, $r(x, t)$, we have

$$f(x, t) \frac{\partial H}{\partial t} = \frac{d\mathcal{V}}{dt} = q_z \Big|_{z=S_x x + H(x)} + r(x, t). \quad (\text{B } 9)$$

Substituting (B 7) in the above expression gives us the governing equation for H :

$$f(x, t) \frac{\partial H}{\partial t} = K_s \frac{\partial}{\partial x} \left(H S_x + H \frac{\partial H}{\partial x} \right) + r(x, t). \quad (\text{B } 10)$$

This equation is equivalent to (2.3) under additional assumptions that groundwater recharge is equal to precipitation — as in Part 2 we ignore the effects of evapotranspiration, and additionally we assume that no overland flow is generated unless the soil becomes fully saturated (i.e. rainfall never exceeds soil infiltration capacity, $r(x, t) \leq K_s$).

B.2. (Region B) Governing equation for saturated zone $H \geq 1$

In the case of the saturated zone, the groundwater height is fixed at $H_g = L_z$. However, the goal is to determine the additional surface water height, $h_s(x, t)$, which is given by solving the Saint Venant equation [eqn (3.3) from Part 2]:

$$\frac{\partial h_s}{\partial t} = \frac{\partial}{\partial x} \left[q_s(h_s) \right] + r(x, t) - I(x, t), \quad (\text{B } 11)$$

where the surface flow, $q_s(h_s)$, is given by the Manning's equation (2.6), and I is the infiltration rate, equal to the negated vertical flow, $-q_z$, at ground level.

In order to determine the vertical flow, q_z , we perform a similar conservation argument to the previous section. First, note that at the interface between subsurface and surface flows, we set continuity of pressure and flow. The first condition allows us to specify the hydraulic head, h_g , at the surface:

$$h_g(x, z, t) = h_s(x, t) \quad \text{at } z = S_x x + L_z. \quad (\text{B } 12)$$

Consequently, we set the integration constant, H , appearing in (B 3) to $H(x, t) = L_z + h_s(x, t)$. Substitution into (B 4) gives:

$$q_x = -K_s \left(S_x + \frac{\partial h_s}{\partial x} \right) \quad \text{for } 0 < z < L_z. \quad (\text{B } 13)$$

We now consider the control volume of groundwater contained in the vertical column $[x, x + \Delta x]$, as illustrated in fig. 10 in Region B. In this case, we have $H_g = L_z$ and so the mass balance equation (B 7) yields

$$q_z \Big|_{z=S_x x + L_z} = -L_z \frac{\partial q_x}{\partial x} = \frac{\partial}{\partial x} \left(K_s L_z S_x + K_s L_z \frac{\partial h_s}{\partial x} \right) = \frac{\partial}{\partial x} \left(K_s L_z \frac{\partial h_s}{\partial x} \right), \quad (\text{B } 14)$$

once we have substituted the expression (B 13) from the groundwater flow, q_x . Thus, we have the required expression for the infiltration rate:

$$I(x, t) = -q_z \Big|_{z=S_x x + L_z} = -\frac{\partial}{\partial x} \left(K_s L_z \frac{\partial h_s}{\partial x} \right). \quad (\text{B } 15)$$

Note that the infiltration is positive if surface water filtrates into the soil, or is negative if groundwater emerges to the surface.

After substituting q_s from (2.6) and infiltration I from (B 15) into (B 11) we get the final surface equation:

$$\frac{\partial h_s}{\partial t} = \frac{\partial}{\partial x} \left(K_s L_z \frac{\partial h_s}{\partial x} + \frac{1}{n_s} \sqrt{S_x + \frac{\partial h_s}{\partial x}} h_s^k \right) + r(x, t). \quad (\text{B } 16)$$

Note that in saturated zone, $H = H_g + h_s$, where $H_g = L_z$ is constant, and hence this equation is equivalent to the governing equation (2.5). Thus, we have derived both cases of the governing equation (2.7) forming the basis of this work.

Appendix C. The drainable porosity function, $f(x, t)$

C.1. On the mean drainable porosity $f(x)$

The drainable porosity function, $f(x, t)$, which occurs in the non-fully saturated regime in (2.3), essentially serves as an *a priori*-unknown placeholder for the vertical flow through the unsaturated layer of soil, as it connects with the fully saturated soil at the depth of $H = H_g$. As discussed in appendix B, it can be formally defined as dV/dH , the volumetric change in groundwater volume for a given change in the height. However, finding this derivative in theory requires solving a two-dimensional Richards equation in the unsaturated zone.

Typically, when the precipitation increases, as in our benchmark scenario, to a constant value $r > 1$, then a characteristic wetting front is observed. This is presented in Figure 11A in Part 2 (and discussed in detail by [Caputo and Stepanjants 2008](#)). The front moves downwards towards the groundwater table, changing soil saturation and eventually leading to the groundwater recharge—this is then interpreted as the term $r(x, t)$. This behaviour is not captured by a standard time-dependent Boussinesq equation or our one-dimensional model.

However, our analysis in sections 6.1 and 6.2 shows that the most important mechanism in which groundwater contributes to the peak flow generation is by extending the saturation zone. Moreover, in appendix F we show that the horizontal groundwater flow is negligibly slow and does not impact the speed with which the groundwater is rising in a short timescale characterising typical rainfalls. This means that the groundwater becomes saturated when the precipitation fills the available drainable volume v_h , *i.e.* after time $t = v_h/r$. The same critical time is predicted by the 1D model by setting constant mean drainable porosity, defined as

$$f(x, t) = f(x) = \frac{v_H(x)}{D(x)}, \quad (\text{C1})$$

and the above choice of mean drainable porosity is one that we use throughout this work.

To summarise, even though setting a time-independent porosity and constant groundwater recharge does not capture the delay the wetting front requires in order to reach the groundwater, it allows the correct prediction of the soil critical time and the resultant peak flows we observe in this work. In case of this model, note that $H(x, t)$ does not represent the exact thickness of the saturated zone that forms groundwater, but rather, it corresponds to the amount of water absorbed by the soil—even if it has not yet reached the saturated zone. Still, this difference in interpretation does not seem to affect the main results obtained in this paper. Formulating this complex system (leading to the drainable porosity) in terms of a 1D PDE facilitates the analysis and computation.

C.2. Computation of mean drainable porosity

Here, we formally derive an expression for the mean porosity given 1D model parameters for the considered benchmark scenario. Firstly, following Richards equation we find the hydraulic head h_g profile above the groundwater table, and use it to evaluate drainable volume for a column of soil of height $D(x)$ above the groundwater table.

We shall note that in the considered case of $\beta_{zx} = L_z/L_x \ll 1$, the leading solution of

two-dimensional Richards equation involves only vertical flow along the \hat{z} axis, as given by (B1). In the scenario considered in this paper, we assume that the system is initially in a steady state for a constant rainfall r_0 . Under these assumptions, we integrate the time-independent version of (B1) to form a first-order nonlinear ODE for pressure head $h_g(\hat{z})$:

$$K_r(h_g) \left(\frac{dh_g}{d\hat{z}} + 1 \right) = \frac{r_0}{K_s}, \quad (\text{C } 2)$$

where the constant of integration, on the right hand-side, has been chosen to match the dimensionless infiltration r_0/K_s , passing through the surface. Let us consider a column of the soil above a groundwater table, we take $h_g \Big|_{\hat{z}=0} = 0$. Given pressure head, we can find saturation $\theta(h_g(\hat{z}))$ following Maulem Van-Genuchten model (C3),

$$\theta(h_g) = \begin{cases} \theta_r + \frac{\theta_s - \theta_r}{(1 + (\alpha h_g)^n)^m} & h_g < 0 \\ \theta_s & h_g \geq 0 \end{cases}, \quad (\text{C } 3)$$

and use it to compute drainable volume and resulting mean drainable porosity (C1),

$$f(x) = \frac{v_H(x)}{D(x)} = \frac{1}{D(x)} \int_0^{D(x)} [\theta_s - \theta(h_g(\hat{z}))] d\hat{z}. \quad (\text{C } 4)$$

Solving (C2) and then integrating (C4) numerically allows us to calculate f .

C.3. Analytic approximations of mean drainable porosity

As an alternative to the integral expression above, let us develop an approximation for v_H based on the assumption that the groundwater table is located near the land surface. Since for $h \rightarrow 0$, $K_r(h) \rightarrow 1$, the leading-order solution for (C2) around $\hat{z} = 0$ satisfies

$$h_g(\hat{z}) \sim \left(\frac{r_0}{K_s} - 1 \right) \hat{z}. \quad (\text{C } 5)$$

Then integrating (C4) with the MvG model (C3) gives:

$$f_1(x) = (\theta_s - \theta_r) \left[{}_2F_1 \left(m, \frac{1}{n}; 1 + \frac{1}{n_s}; \left(-a \left(\frac{r_0}{K_s} - 1 \right) D(x) \right)^n \right) - 1 \right], \quad (\text{C } 6)$$

where ${}_2F_1$ is a hypergeometric function. One can also find the leading order approximation of (C6) for $D \ll 1$, which yields:

$$f_2(x) = \frac{m}{n+1} (\theta_s - \theta_r) \left[- \left(\frac{r_0}{K_s} - 1 \right) \alpha D(x) \right]^n. \quad (\text{C } 7)$$

However, approximation (C6) is more accurate. Functions (C6) and (C7) are compared with full numerical solution in fig. 11.

Appendix D. Derivation of steady-state overland flow for $\mu \rightarrow \infty$

The steady state for the saturated zone is given by equation (5.1b):

$$1 + \sigma \frac{\partial h_0}{\partial x} + \mu h_0^k = \rho_0(1 - x). \quad (\text{D } 1)$$

where we used $h_0(x) = H(0) - 1$ to represent surface water height.

As we have noted previously, our regime of interest is where μ is large. It is convenient to re-scale via $x = aX$, where a was defined as a size of saturated zone, so that the domain

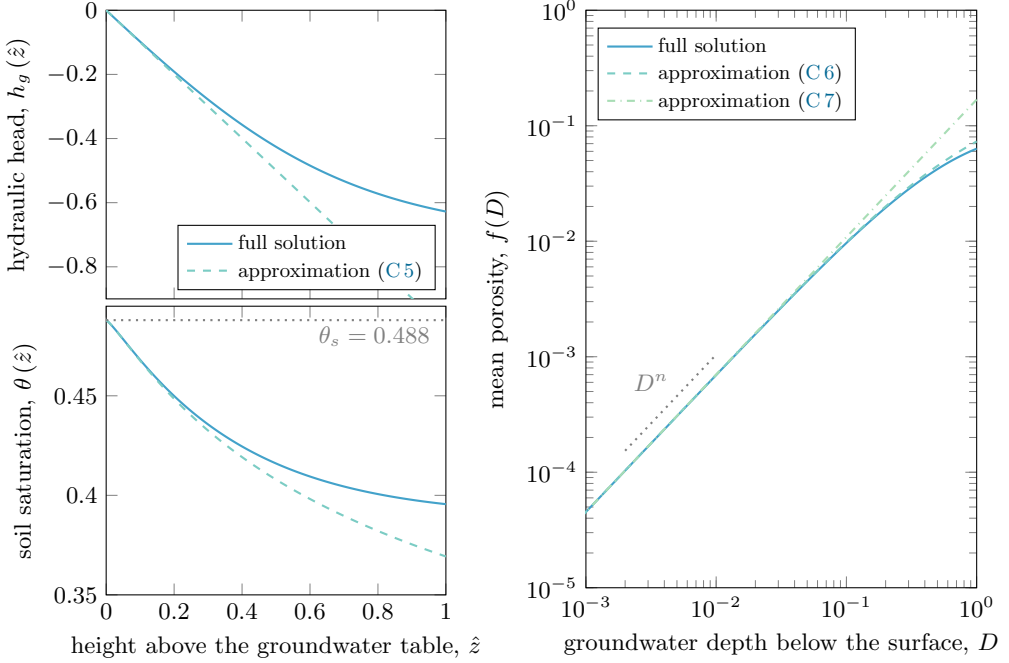


Figure 11: On left: Initial vertical profile of the hydraulic head h_g and corresponding saturation θ in a column of soil. On right: Dependence of mean porosity $f = \frac{\theta_h}{D}$ on the depth of the groundwater below the surface. As shown, approximations (C5)-(C7) are accurately describing soil properties close to the groundwater table. We used MvG parameter values from previous part of our work, i.e. $\alpha = 3.367\text{m}^{-1}$, $\theta_s = 0.388$, $\theta_R = 0.115$ and $n = 1.282$.

is fixed in $X \in [0, 1]$. In the limit $\mu \rightarrow \infty$, we anticipate from dominant balance that the overland flow is small, $h_0 \rightarrow 0$, and hence we re-scale $h_0 = \mu^{-1/k}g(X)$ in order to balance the third term with the right-hand side of (D 1). With the boundary conditions (4.3a,c), this gives

$$\frac{\text{Pe}^{-1}}{a} \frac{\partial g}{\partial X} + g^k = \rho_0(1 - aX) - 1, \quad (\text{D } 2a)$$

$$g'(0) = 0 \quad \text{and} \quad g(1) = 0. \quad (\text{D } 2b)$$

In (D 2a), for convenience, we have defined the small parameter,

$$\text{Pe}^{-1} = \frac{\sigma}{\mu^{1/k}} \ll 1,$$

which, according to table 1 we estimate it to be $\text{Pe}^{-1} \approx 10^{-5}$. As we shall see, the asymptotic analysis as $\text{Pe}^{-1} \rightarrow 0$ involves the analysis of an outer solution, where $0 \leq X < 1$, and an inner solution with a boundary layer, where $X \rightarrow 1$.

In the outer region, we expand the solution and contact line as

$$g(X) = g_0(X) + \text{Pe}^{-1}g_1(X) + \dots \quad \text{and} \quad a = a_0 + \text{Pe}^{-\gamma}a_1 + \dots \quad (\text{D } 3)$$

where $\gamma > 0$ and is to be determined later. Then we develop the following leading-order

approximation of the outer surface water height via (D 2a),

$$g(X) \sim g_0(X) = [\rho_0(1 - a_0X) - 1]^{1/k}. \quad (\text{D } 4)$$

The above outer expansion exhibits an infinite gradient, possibly before the contact line is reached, at the point $X = (1 - \rho_0^{-1})/a_0$. However, we show below that a_0 is such that this point corresponds to $X = 1$.

In order to develop the solution within the boundary layer, we consider re-scaling

$$g(X) = \text{Pe}^{-\beta} \hat{G}(\hat{X}) \quad \text{and} \quad X = 1 - \text{Pe}^{-\alpha} \hat{X},$$

with α , β , and γ from (D 3) to be determined. Applying these transformations to (D 2a) gives:

$$\begin{aligned} \text{Pe}^{-(1+\beta-\alpha)} \left[-\frac{1}{a_0} \frac{\partial \hat{G}}{\partial \hat{X}} \right] + \text{Pe}^{-k\beta} \left[\hat{G}^k \right] = \\ \left[\rho_0(1 - a_0) - 1 \right] + \text{Pe}^{-\alpha} \left[\rho_0 a_0 \hat{X} \right] - \text{Pe}^{-\gamma} \left[\rho_0 a_1 \right] + o(\text{Pe}^{-\alpha}) \end{aligned} \quad (\text{D } 5)$$

The balance of Pe terms is achieved for $1 + \beta - \alpha = k\beta = \alpha = \gamma$, which corresponds to $\alpha = \gamma = k/(2k - 1)$ and $\beta = 1/(2k - 1)$. The equation (D 5) for the leading $\mathcal{O}(1)$ term is $\rho_0(1 - a_0) - 1 = 0$ and hence this gives us an estimate for the leading-order contact line position,

$$a \sim a_0 = 1 - \frac{1}{\rho_0}. \quad (\text{D } 6)$$

Indeed, this confirms that the leading-order outer solution, (D 4), predicts an infinite gradient as $X \rightarrow 1$. In order to derive an approximation for the gradient of the surface water height near the contact line, we must proceed to the next order in the inner region.

The equation (D 5) at $\mathcal{O}(\text{Pe}^{-\frac{k}{2k-1}})$ yields

$$-\frac{1}{a_0} \frac{\partial \hat{G}}{\partial \hat{X}} + \hat{G}^k = \rho_0 a_0 \hat{X} - \rho_0 a_1, \quad (\text{D } 7a)$$

along with the two boundary conditions of

$$\hat{G}(0) = 0 \quad \text{and} \quad \hat{G}(\hat{X} \rightarrow \infty) \sim (\rho_0 - 1)^{1/k} \hat{X}^{1/k}. \quad (\text{D } 7b)$$

The second boundary condition above corresponds to the inner limit of the outer solution (D 4). The above first-order ODE, together with two boundary conditions, forms a boundary-value-problem with eigenvalue a_1 . It cannot be solved analytically. In any case, if desired, the above problem can be computed numerically, and it would yield the correction to the contact line, $a_1 = a_1(\rho_0)$.

Notice finally that the gradient of h_0 at $x = a$ can now be estimated directly from equation (D 1). Since $h_0(a) = 0$, we have, using the expansion (D 3),

$$\left. \frac{\partial h_0}{\partial x} \right|_{x=a} = \frac{\rho_0(1 - a) - 1}{\sigma} \sim \frac{\rho_0(1 - a_0) - 1 - \rho_0 a_1 \text{Pe}^{-\gamma}}{\sigma} = -\frac{\rho_0 a_1}{\sigma} \text{Pe}^{-\gamma}. \quad (\text{D } 8)$$

For Manning's law, $k = 5/3$, so $\gamma = k/(2k-1) = 5/7$. Hence, we expect the gradient to be $dh_0/dx = \mathcal{O}(\text{Pe}^{-5/7})$ while the contact line position equally satisfies $a - a_0 = \mathcal{O}(\text{Pe}^{-5/7})$. These two scaling laws are confirmed by solving the boundary value problem given by equation (D 2a) numerically and transforming it back to the original variables (see fig. 12).

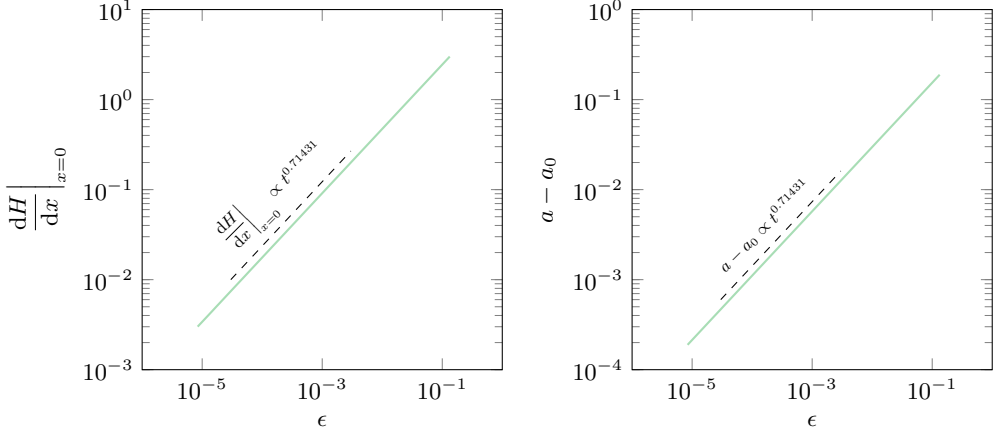


Figure 12: The size of the saturation zone relative to its first order approximation $a - a_0$ (on left) and the gradient of H at this point. The results were obtained by solving eqn (D1). The fitted power law is consistent with the theoretical exponent $\gamma = 5/7 \approx 0.7142(86)$.

Appendix E. Derivation of the initial groundwater table for $\sigma \rightarrow 0$

Here we find a leading-order solution for ODE (5.6) under the limit $\epsilon = \sigma \rightarrow 0$:

$$\epsilon \frac{dH_0}{dx} = \frac{\rho_0(1-x)}{H_0(x)} - 1, \quad \text{for } x \in [a_0, 1], \quad (\text{E1})$$

with a boundary condition $H_0(a_0) = 1$, and where $a(t) \sim a_0$ is the leading-order contact line position as $\text{Pe} \rightarrow \infty$. Expanding H_0 in powers of ϵ , we obtain the approximation,

$$H_0(x) = \rho_0(1-x) + \rho_0\epsilon + \mathcal{O}(\epsilon^2). \quad (\text{E2})$$

This solution does not satisfy the boundary condition at $x = a_0$. For $x \rightarrow a_0$, we develop an inner expansion by re-scaling $x = a_0 + \epsilon X$ and $H_0(x) = g(X)$. The ODE now becomes

$$\frac{dg}{dX} = \frac{\rho_0(1-a_0-\epsilon X)}{g(X)} - 1, \quad \text{for } X > 0, \quad (\text{E3})$$

with $g(0) = 1$. Solving now to the first two orders, we have,

$$g(X) = 1 + \epsilon\rho_0(1 - e^{-X} - X) + \mathcal{O}(\epsilon^2), \quad (\text{E4})$$

where we have used $a_0 = 1 - 1/\rho_0$ from (5.5).

The composite solution is obtained by adding outer and inner asymptotic expansions from (E2) and (E4), respectively, and subtracting their common part. The final result, to two orders of accuracy, is the following approximation:

$$H_0(x) = \rho_0 \left(1 - x + \epsilon - \epsilon e^{-\frac{x-a_0}{\epsilon}} \right) + \mathcal{O}(\epsilon^2). \quad (\text{E5})$$

After replacing ϵ with σ , we obtain the solution (5.7) stated in the main text.

Appendix F. Derivation of groundwater solution for $t \rightarrow 0$ and $\rho \rightarrow \infty$

We provide additional details for the early-time analysis of section 6.1, particularly in connection with the boundary-layer asymptotics. Consider equation (4.2b) for the

unsaturated zone $H < 1$:

$$f(x) \frac{\partial H}{\partial t} = \frac{\partial}{\partial x} \left(\sigma H \frac{\partial H}{\partial x} + H \right) + \rho. \quad (\text{F } 1)$$

As noted in §6.1, we consider the initial condition, $H(x, t = 0) = H_0(x; \rho_0)$, to be the steady-state response of the system to a long-time precipitation rate, ρ_0 . That is, the initial groundwater solution satisfies (5.6),

$$(\sigma H_0 H'_0 + H_0)' + \rho_0 = 0, \quad (\text{F } 2)$$

subject to the boundary conditions (4.3b,d) in §5, i.e.

$$H(x = a(t)) = 1 \quad \text{and} \quad \left. \left(\sigma H \frac{\partial H}{\partial x} + H \right) \right|_{x=1} = 0 \quad (\text{F } 3)$$

Let us consider the short-time behaviour of the time-dependent equation by $t = \epsilon t'$, $H(x, t) = H_0(x) + \epsilon H'(x, t)$ with $\epsilon \ll 1$. Then (F 1) becomes:

$$f(x) \frac{\partial H'}{\partial t'} = \rho - \rho_0 + \epsilon \frac{\partial}{\partial x} \left(\sigma H_0 \frac{\partial H'}{\partial x} + \sigma H' \frac{\partial H_0}{\partial x} + H' \right) + \mathcal{O}(\epsilon^2). \quad (\text{F } 4)$$

The small-time groundwater solution, correct to two orders, is then

$$H(x, t) = H_0(x; \rho_0) + \left[\frac{\Delta \rho}{f(x)} \right] t + \mathcal{O}(t^2), \quad \text{as } t \rightarrow 0 \text{ with } x > a(t) \quad (\text{F } 5)$$

where $\Delta \rho \equiv \rho - \rho_0$. Thus, we see that (F 5) predicts that the groundwater height increases linearly with time by an amount proportional to the sudden impulse of rain (or rather, its difference $\Delta \rho$).

However, the above asymptotic solution assumes that $x - a(t) = \mathcal{O}(1)$, and indeed it fails to account for the fact that $H = 1$ when $x = a(t)$. We must consider it to be an *outer* solution, valid away from $x = a(t)$. A comparison between the outer approximation (F 5), and the full solution is shown in fig. 6(a). In the case of the fully-coupled surface-subsurface flow, the solution of the PDE diverges from the outer solution (F 5) within a small boundary layer around the saturated/unsaturated zone interface.

The size of the boundary layer tends to zero as $\rho \rightarrow \infty$. This is tested as follows. We compute the full PDE model (2.8a) and find the place where $H(x_{\text{numeric}}) = 1$. We can then estimate the boundary layer thickness by finding the difference between x_{numeric} and $x_{\text{approx}} = 1 - 1/\rho$, which is the leading-order (outer) approximation of $a(t)$. As fig. 13 demonstrates, it depends both on time t and precipitation represented by ρ .

The above is confirmed via a dominant balance. Let $x = a + \delta x'$. Then eqn (F 4) becomes:

$$f(x) \frac{\partial H'}{\partial t'} = \rho - \rho_0 + \frac{\epsilon}{\delta^2} \frac{\partial}{\partial x'} \left(\sigma H_0 \frac{\partial H'}{\partial x'} + \sigma H' \frac{\partial H_0}{\partial x'} + \delta H' \right) + \mathcal{O}(\epsilon^2) \quad (\text{F } 6)$$

The diffusion terms become significant and balance the precipitation, ρ , when $\epsilon/\delta^2 \sim \Delta \rho$. Then the thickness of the boundary layer is on the order of $\delta = \epsilon^{1/2} \Delta \rho^{-1/2}$, i.e. it increases proportionally to $t^{1/2}$ and $\Delta \rho^{-1/2}$. These trends are confirmed in fig. 13.

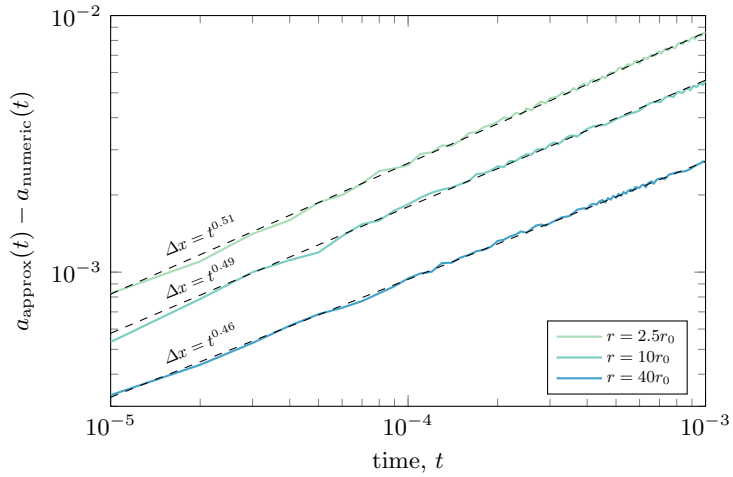


Figure 13: Difference between the location of saturated zone front obtained by solving PDE (2.8a) and obtained using the leading term outer solution (F5) for rainfalls with three different precipitation rates.